NUMERICAL SIMULATION OF FLOW PHENOMENA IN ROTATING VISCOMETERS

By

M. Madan

DEPARTMENT OF MATERIALS AND METALLURGICAL ENGINEERING

Indian Institute of Technology, Kanpur

APRIL. 2004

NUMERICAL SIMULATION OF FLOW PHENOMENA IN ROTATING VISCOMETERS

A Thesis Submitted

In Partial Fulfillment of the Requirements

For the Degree of

MASTER OF TECHNOLOGY

By

M. Madan

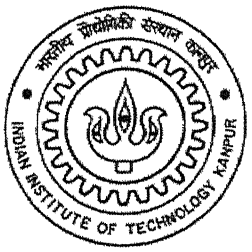

DEPARTMENT OF MATERIALS AND METALLURGICAL ENGINEERING

INDIAN INSTITUTE OF TECHNOLOGY, KANPUR

APRIL, 2004

CERTIFICATE

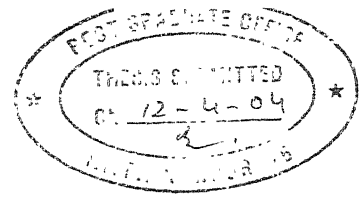

This is to certify that the present work **"NUMERICAL SIMULATION OF FLOW PHENOMENA IN ROTATING VISCOMETERS"** has been carried out by M. Madan (Roll no: Y120610) towards his M. Tech. dissertation under my supervision and this has not been submitted elsewhere for a degree.

April 12, 2004

(*Prof. Dipak Mazumdar*)
Deptt. of Materials and Metallurgical Engineering
Indian Institute of technology, Kanpur

ACKNOWLEDGEMENT

I take the opportunity to express my sincere gratitude and regards to ***Prof. Dipak Mazumdar*** for his astute guidance, invaluable suggestions and discussions and freedom to work. His nature of hard work, enthusiasm and integral view on research provided me a deep impression on him.

I also thank ***Prof. S.C. Koria*** for his suggestions and kindly words which helped me in improving my confidence. I also thank other Professors for their direct and indirect assistance.

I cordially thank all my labmates: ***Mr. Mukesh Bharadwaj, Mr. Amitava Paul, Satish, Jayant, Emila, Surendra*** and ***Sujay*** for their timely help and made my stay pleasant.

I am deeply indebted to all my friends, who made my stay at IIT Kanpur a memorable one. I will never forget the moments I spent with ***Sankar, Chelladurai, Rajasekhar, Ganesh Babu, Muthu, Murugan, Pugal, Suresh, Sivabalan, Ramesh, Venkateswaran*** and ***Bhagyaraj.***

I am also thankful to ***Sharmaji*** and all the technical staff for their direct and indirect help towards my project.

Financial assistance received from IIT Kanpur and Ispat Industries, Mumbai is gratefully acknowledged.

M. Madan
Indian Institute of Technology
Kanpur

CONTENTS

ABSTRACT

Mathematical modelling is used in steelmaking to study various phenomena as the opacity and high temperature of operation limits direct visualization. Computational Fluid Dynamics (CFD) enables us to simulate steelmaking conditions realistically and scientific visualization thus provides us necessary information on reactor efficiency and process dynamics.

In the present work, mathematical modelling is applied to study the flow in the annulus of two concentric rotating cylinders as in the case of rotating viscometer (inner cylinder rotating). The commercial CFD package FLUENT is used to simulate the flow phenomena. The simulations were carried out with the model configurations as three dimensional, steady state, laminar, isothermal and with constant density and viscosity. The shear stress values were computed and compared with the experimental values reported in the literature. Two different viscometer configurations were mathematically modelled. It was found that very reasonable to excellent agreement exists between experimental and computed shear stress. The computational results justified the present approach of uni-dimensional flow theory coupled with calibration data towards estimation of melt viscosity via rotating viscometers. In addition to these, design of viscometers was also investigated computationally and the role of crucible taper, the clearance distance between the rotating cylinders etc. were investigated computationally. It was found that tapering of the outer cylinder was not critical to the shear stress generated at the surface of the rotating cylinder. Similarly, there is a critical distance of clearance between the concentric cylinders such that the outer cylinder has negligible impact on shear stress/ torque measurement. In all cases, grid independent solutions were generated prior to making any comparison between experimental and computed results.

LIST OF FIGURES

Page No

LIST OF TABLES

CHAPTER I

INTRODUCTION

1.1 INTRODUCTION TO THE THESIS

Model is a term that represents and predicts a real phenomenon and is carried to study a phenomenon, which cannot be possibly studied in-situ or in real time because of the very nature of the system and the surrounding. For example, it is hazardous and difficult to study the flow pattern and heat transfer effects in the steel making furnaces because of its high temperature of operation and large size. Also, we cannot view the happenings inside the furnace to have precise knowledge about the phenomena under investigation. This makes it difficult to investigate the process dynamics and optimize the underlying process. As a result, modelling has been extensively used nearly in all areas of iron and steel making, as the temperature of operations exceeds well above 1600°C. Three different approaches have been applied commonly [1] and these include:

1. Physical Modelling.
2. Mathematical Modelling and
3. Pilot Plant Modelling.

Physical modelling is an experimental investigation in a reduced scale model often using an altogether different fluid. If the physical model employs water, it is termed as aqueous or water model. A scaled down model (based on various state of similarity) is made to represent the real process. The materials used for the creating the models need not be as same as full-scale. The primary goal of the physical models is to measure the characteristics of the real system inexpensively and conveniently. Typical examples of physical modelling include the modelling of argon-stirred ladles using the air-water

system, the use of flowing water in Plexiglas containers to represent the tundish systems in continuous casting and the water model of the mold in continuous casting system. Many experiments (on mixing, mass transfer, heat transfer, subsurface trajectories etc.) are commonly conducted in the model and the resulting informations are extrapolated to full-scale systems. Physical model studies may have different objectives. For example,

1. Measurements taken in rigorously constructed physical models which satisfy similarity criteria, including geometry, kinetic and dynamic similarities may be readily scaled to obtain quantitative information regarding the behaviour of the prototype.
2. The measurements may also be used in a corresponding physical system to verify or test a mathematical model. The latter may in turn be used to predict the behaviour of the real operating system.

The use of Plexiglas as containing material and water as working fluid provides a very useful insight into the behaviour of the system, which in turn gives excellent guidance regarding possible design changes with few additional costs. But these models suffer from serious drawbacks: The small-scale models do not always simulate all the features of the full-scale equipment. The important features such as combustion or boiling cannot be simulated in scaled down models. The non-isothermal behaviour cannot be represented accurately in the physical models. There is no general rule for extrapolating the results under such circumstances. Finally, the measuring instruments are also not free from errors.

A mathematical model is a set of algebraic or differential equations, which quantitatively represent a system or process. The system is represented in set of mathematical equations which is solved for the requisites of the problem. The strength of the mathematical model is that it links the operating process to fundamental principles and thereby provides a basic understanding of the process [2]. The main types of mathematical models are: Mechanistic models and Empirical models. The mechanistic models based on basic physical or chemical law such as thermodynamic equilibria,

chemical kinetics, conservation of mass, momentum and energy, etc. owing to their fundamental nature, these models tend to have general validity. In contrast, empirical models based on direct observations of a particular system and not on fundamentals. These models tend to be more specific to a set of operating conditions.

The main advantages of the mathematical models are: cheap when compared to setting up a physical model or a pilot plant, takes less time, gives complete and detailed information about the problem, its ability to simulate realistic conditions and it s ability to simulate ideal conditions. The drawbacks of the mathematical model are: validation of the model with the experimental data is required as there is uncertainty about the extent to which the computed results would agree with reality.

The pilot plants are replicate of the full scale installations on a smaller scale. These represent all the functionalities of the full scale models and in that sense, it is different from the physical models. The usual scale of the pilot plants will be 5 – 15% of the prototype and 30% for the demonstration plants, which also comes under same category. The pilot plants are generally applied to:

1. New process development where available tools are inadequate for reliable design of a full-scale plant.
2. Existing processes for which it is often impossible to perform measurements on a full-scale unit.
3. Provision of product material for market analysis.

The construction and operation of the real process is the main advantage of the pilot plant. The draw backs of the pilot plant are: highly expensive, large time consumption and more need of materials and man power. The pilot plants are used mainly as final step in the modelling after doing physical and mathematical modelling.

As the three modelling types having their own advantages and disadvantages, the choice of prediction is made by combining all the types [3]. The phenomenon is

investigated experimentally and then mathematically. The changes in the design of the model are made wherever needed and finally the pilot plant model is made before putting it into use. The Figure 1.1 shows the schematic diagram of three essential components of successful investigation.

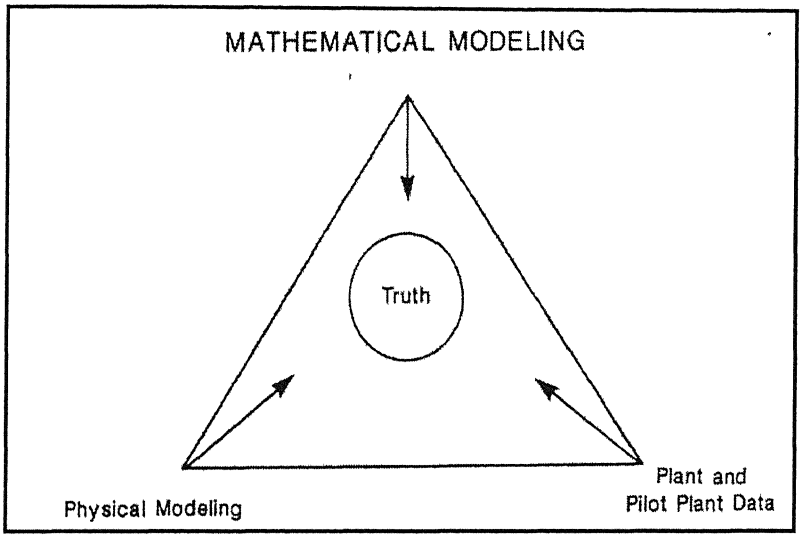

Figure 1.1: Three essential components of successful investigation

1.2 LITERATURE REVIEW: MATHEMATICAL MODELLING IN STEELMAKING

In this section, introductory remarks on mathematical modelling are included and a brief description on the application of CFD to steelmaking is presented. A mathematical model is a set of equations, which may used to represent and predict a certain phenomena. It is certainly different from law as the relationship employed may not be quite exact and the predictions derived from them may only be approximate. The main roles of mathematical model in materials processing are [3]: process control, process optimization, planning and interpretation of measurements and a link to artificial intelligence. This is illustrated schematically in Figure 1.2.

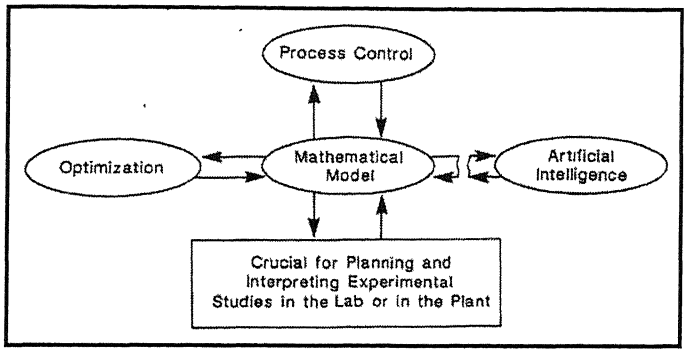

Figure 1.2: The role of mathematical models in materials processing

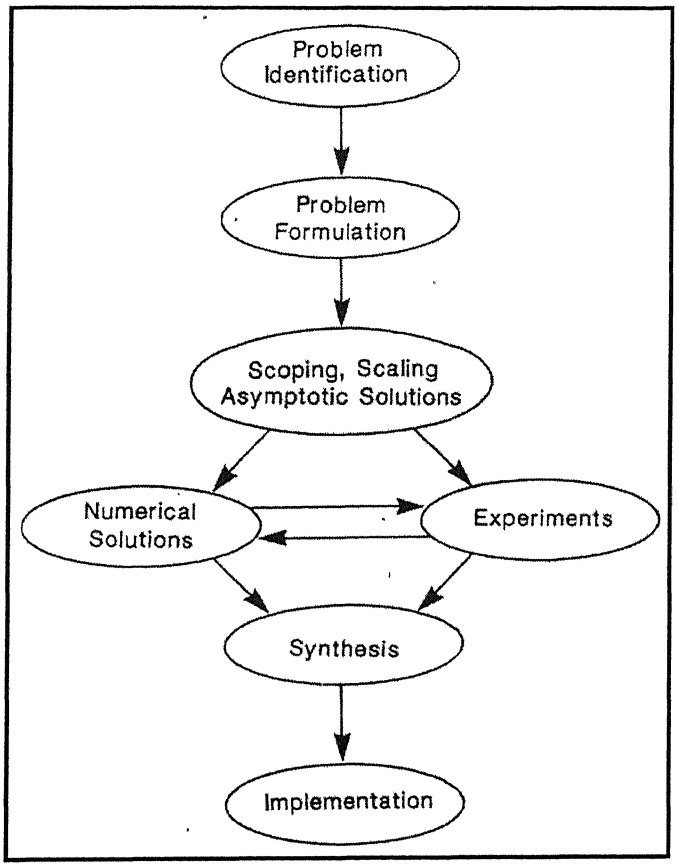

Figure 1.3: General methodology of mathematical model development

A mechanistic mathematical model is developed by following a sequence of steps. Figure 1.3 shows the steps involved in the development of a mathematical model. The

first step, problem identification is the most important step in model development as the problem is hardly ever presented to the investigator in a defined form. The formulation of the problem is done once the problem is identified. The next step is scaling, scoping and order-of-magnitude analysis in which the behaviour of the system i.e. the time scale, velocity scale of the problems etc. are studied. The next step involves parallel activities on numerical solutions and experimentations. Numerical solution of governing equations (which are often differential equations) involve various types of technique including finite element, finite difference, finite volume methods etc. The final step however, is the synthesis which leads to the development of a quantitative understanding of the system. The implementation of the model study program output may involve a decision whether to proceed with a development project or to modify the existing operation or to change the system itself. The key point is, one must re-emphasize regarding the flowchart that once a problem is identified, any investigation should start with calculation first, and then use the flowchart as a framework for planning experimental and computational programs to be pursued in an interactive manner.

In the early days of modelling, the models were custom made which were drawn from the first principles and consideration of elementary control volumes. But in modern times, the models can be directly obtained from preceding relevant studies. Many times analogous models/solutions are readily available together with inexpensive hardware and a wide range of software packages. To-day many models can be readily derived from the corresponding building blocks which are given in Table 1.1. In mathematical modeling of a given phenomena, the physical situation involved may be further divided between well understood and less understood [3] phenomena. For example, the vertical gas injection (a), horizontal gas injection (b), gas jet impinging on a melt (c), induction melting and stirring (d), submerged Arc welding (e) and gas flow through packed bed (f) are examples for well understood phenomenon given in Figure 1.4. The examples for less understood phenomena are atomization of liquid metal stream by gas jet (a), Mechanical stirring of liquid metals (b), Mold filling (c), Emulsification at a slag – metal interface (d) and Surface waves with liquid metals (e) which is shown in Figure 1.5.

Component	Application	Remarks
Navier-Stokes Equations	Fluid flow	Complex vector-tensor manipulation
Fourier's Law	Heat conduction	Relatively simple, more complex if phase change is involved
Fick's Law	Diffusion	Simple for one component, very complex for multi-component systems
Convective transport	Heat and mass transfer	Combines fluid flow, heat and/or mass transfer
Maxwell's equations	Electrodynamics, MHD	Very complex problems
Thermodynamics	Equilibria phase diagrams	Often routine calculations
Kinetics	Rate predictions	Needs experimental inputs
Constitutive relationships	Deformation processing	Very complex, needs realistic input

Table 1.1: Building blocks of Mathematical model

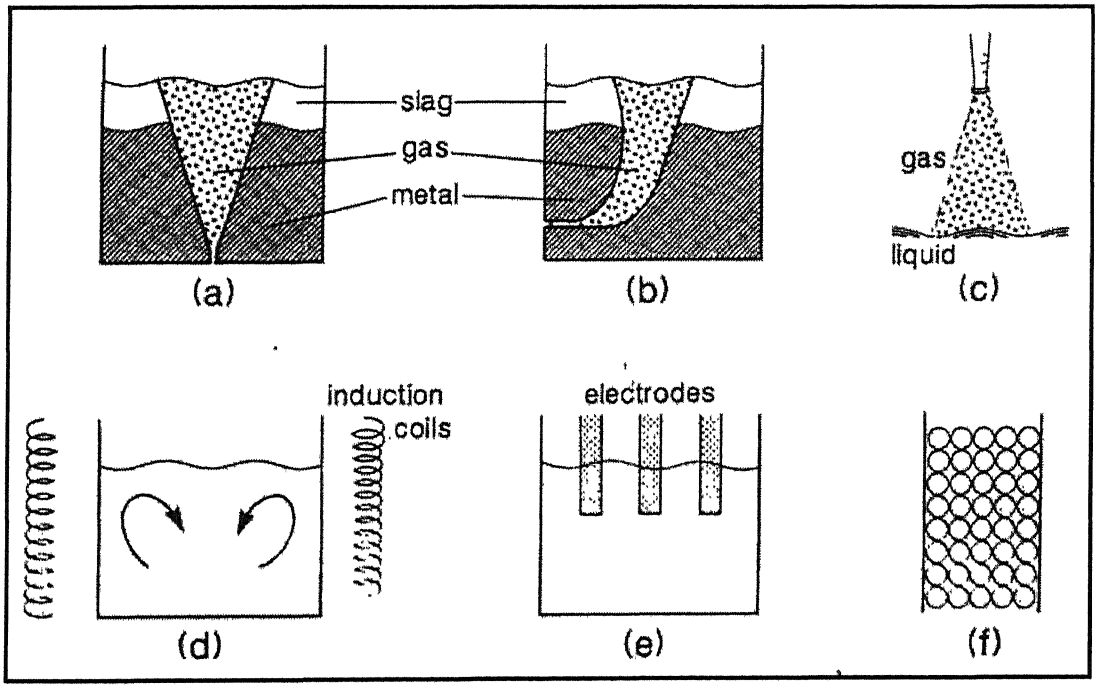

Figure 1.4 (a – f): Some of the well studied physical situations in metallurgy

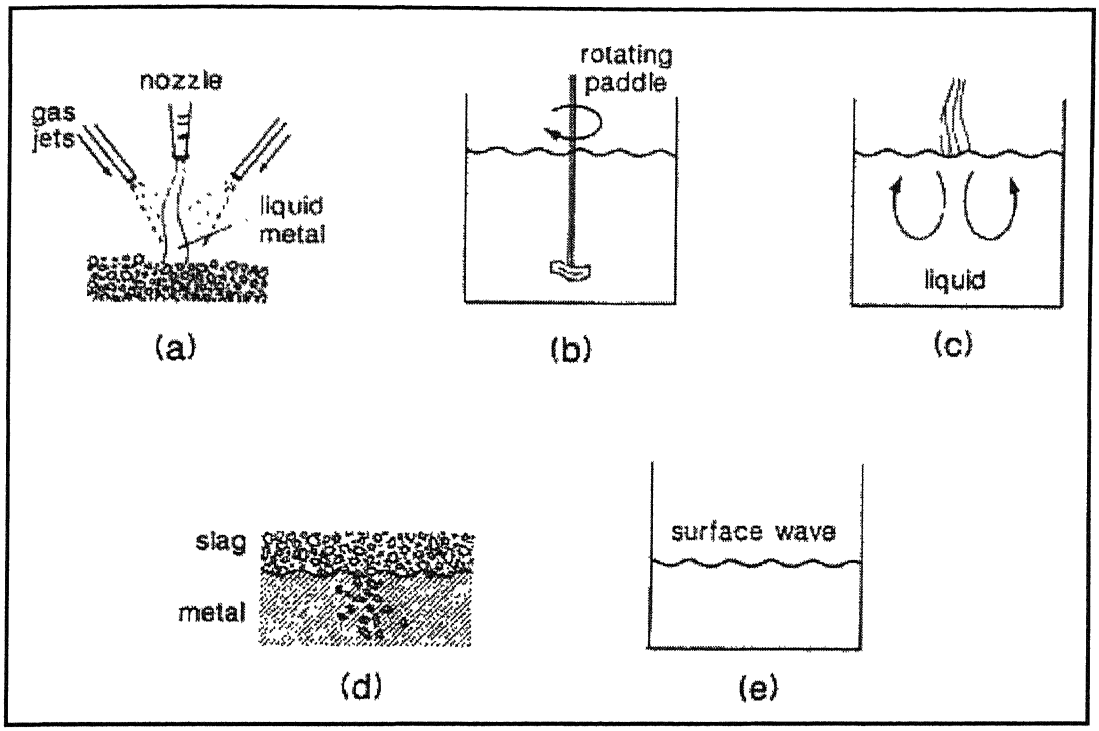

Figure 1.5 (a – e): Some of the less understood physical situations in metallurgy

The recent developments in the field of the mathematical models are introduction of extremely efficient hardware and software. Thus the cost of carrying out a given calculation has been drastically decreased by the introduction of efficient computing machines and powerful software packages. Consequently, transient, three dimensional, multiphase flow simulations has become amenable in the present time. The usefulness of the computer has become more relevant due to their tremendous speed of performing number crunching. In the range of the hardware's, from simple workstations to massive parallel processors, the choice depends on the user and the severity of the problem. For example, mini computers or workstations are enough for doing the two- dimension, laminar flow problems in simple geometry. For doing complex calculations like three-dimension, turbulent, transient and multiphase problems, the needs of super computers or parallel processors are necessary. The software's used for carrying out computations could be either custom made of the available commercial software packages. Availability of commercial software packages (viz., FACT, FLUENT, PHOENICS, FLOW 3-D etc.) has made life of modelers much simpler and to day [4], it is possible to

carry out remarkably complex calculations in many engineering systems with the aid of these software packages extremely efficiently. A partial list of readily available software's is given in Table 2.1. These are applied in a variety of fields [5] including the Aerospace, Automotive, Chemical, Combustion, Electronics, Marine, Metallurgy, Nuclear, Petroleum, Power, Radiation, etc.

With the popularity of CFD (Computational Fluid Dynamics) the steel manufacturing area has been improving a lot by providing a better understanding of the underlying process dynamics [6]. CFD provides detailed performance assessment and therefore, reduces the need for costly experimentation. Using CFD, manufacturing process can be optimized from both quality and cost standpoint. Some of the examples of the use of CFD in the steelmaking areas include: ladle metallurgy, tundish, continuous casting, furnace modelling, etc. The summary of the use of CFD analysis of some of the key steelmaking operations are given in the Table 2.2.

Sl. No	Investigators	Year	Nature of the problem		Software
			Physical	Computational	
1	Salcudean and Guthrie [7]	1978	Tapping of a furnace into a holding ladle	Transient, 3-D turbulent flow	Developed in house
2	Elkaddah and Szekely [8]	1981	Desulphurization in a gas stirred ladle	Steady state, Axisymmetric, turbulent flow	Developed in house
3.	Salcudean and coworkers [9]	1985	Mixing in a gas stirred bath	Steady/unsteady, 3-D single phase turbulent flow	Developed in house
4	Mazumdar and Guthrie [10]	1986	Fluid flow & mixing in CAS process	Steady, axisymmetric turbulent flow	TEACH T
5	Boysan and Johanses [11]	1987	Bubble trajectories and two phase flow in a gas stirred bath	Steady state, axisymmetric, two phase turbulent flow	Developed in house
6	Scwarz and Turner [12]	1988	Fluid dynamics in CAS method	Steady state, axisymmetric, two phase turbulent flow	PHOENICS
7	Illegbussi and Szekely [13]	1989	Tracer dispersion in a tundish	Steady/unsteady, 3-D turbulent flow	PHOENICS
8	Turkoglu and Farouk [14]	1991	Flow and mixing in a gas stirred bath	Steady, axisymmetric, two phase turbulent flow	PHOENICS
9.	Chakraborty and Sahair [15]	1992	Flow and thermal energy transport in tundish	Steady state, 3-D, turbulent flow	Developed in house
10.	Ishi and coworkers [16]	1996	Magneto hydro-dynamics in continuous casting	Steady, 3-D turbulent flow	FLUENT
11	Hsiao and coworkers [17]	1998	Fluid flow in steelmaking tundish	Steady state, 3-D, turbulent flow	CFX-4
12	Bai and Thomas [18]	2000	Fluid flow through slide gate nozzle	Steady state, 3-D, turbulent flow	FLUENT/ CFX-4
13	Morales and coworkers [19]	2003	Fluid flow in continuous casting mold	Transient, 3-D, turbulent flow using LES	Unknown

Table 1.2: Summary of CFD study in steelmaking

Having given the background information, in the following section, two examples are discussed in relatively more detail so as to illustrate the potential and applicability of mathematical modeling/CFD in steelmaking.

The study of gas injection during bottom stirring via three-dimensional numerical simulation has been carried out via both Lagrangian and Eulerian models [20]. A comparison is made between the predicted and experimental flow pattern derived from a scaled water model. The velocity distribution curves for measured (a), Lagrangian model (b) and Eulerian (c) are respectively shown in Figure 1.6. There the Lagrangian model is shown to provide better agreement with measured data than the Eulerian model, as far as the velocity distributions along the central plane is concerned (see Figure 1.7). One may note here that the former model has more advantages in term of simplicity, ability to accommodate changes in bubble size due to coalescence and minimal computational efforts.

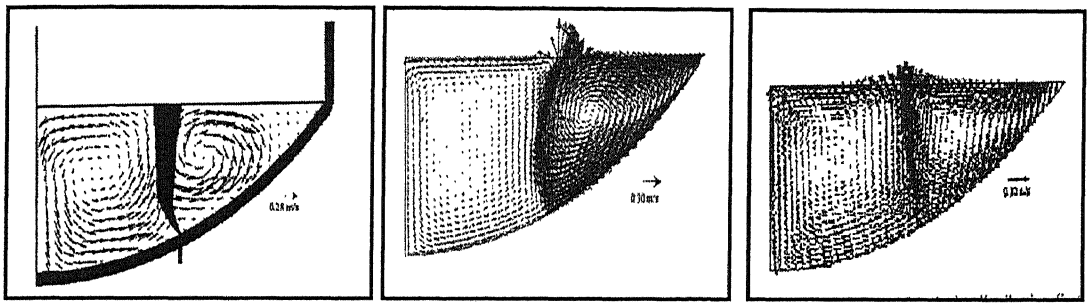

(a) (b) (c)

Figure 1.6 (a, b and c): Velocity distributions in gas stirred ladles

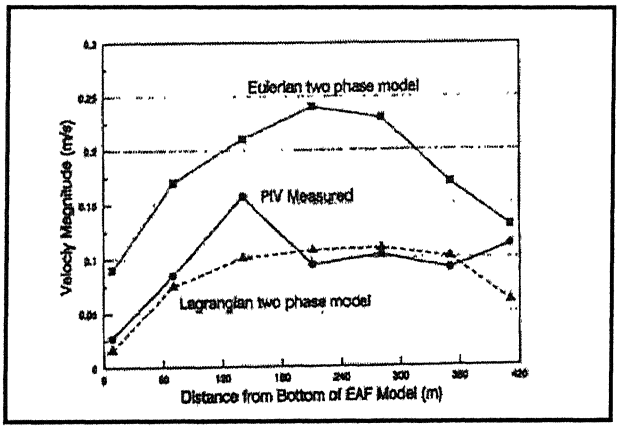

Figure 1.7: Measured and computed velocity along the central plane of the gas stirred ladle (Fig. 1.6)

The CFD analysis of the three-dimensional flow field and tracer dispersion study in the water model of an industrial tundish was carried out to arrive at optimal tundish design and optimal location of flow modifiers such as dams, weirs and baffles [3]. Figure 1.8 shows the tundish used for numerical simulation while Figure 1.9 shows the velocity field at the centre plane for different configurations. The corresponding tracer dispersion curves for the different flow configurations are shown in Figure 1.10. Referring to Fig.1.9, it is seen that configuration (a) with no flow control device tend to show a strong recirculating flow occupying a significant part in the tundish. Configuration (b), on the other hand, shows improvement in the flow pattern which has a dam and a weir. Configuration (c) illustrates the effect of placing a strong magnetic field on the tundish. Such trends in computed results appear to fall on line with the corresponding tracer dispersion curves. The effect of short circuiting and by-passing is shown clearly in (a) and this is reduced to a considerable extent with the use of dams and weirs (b). These figures also show that plug flow condition is approached only through the use of externally imposed magnetic field.

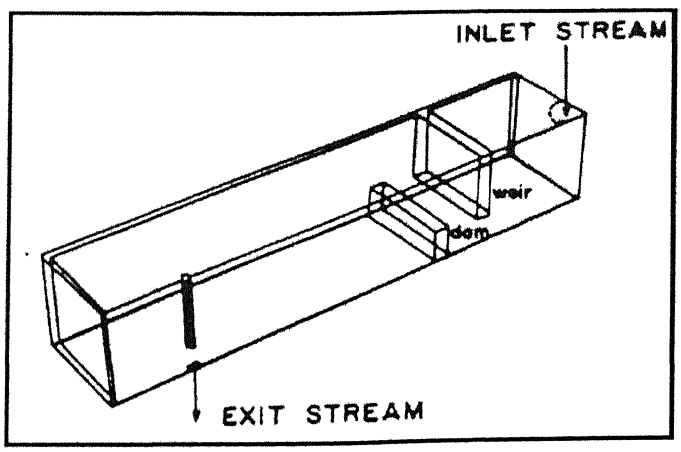

Figure 1.8: Schematic diagram of a tundish

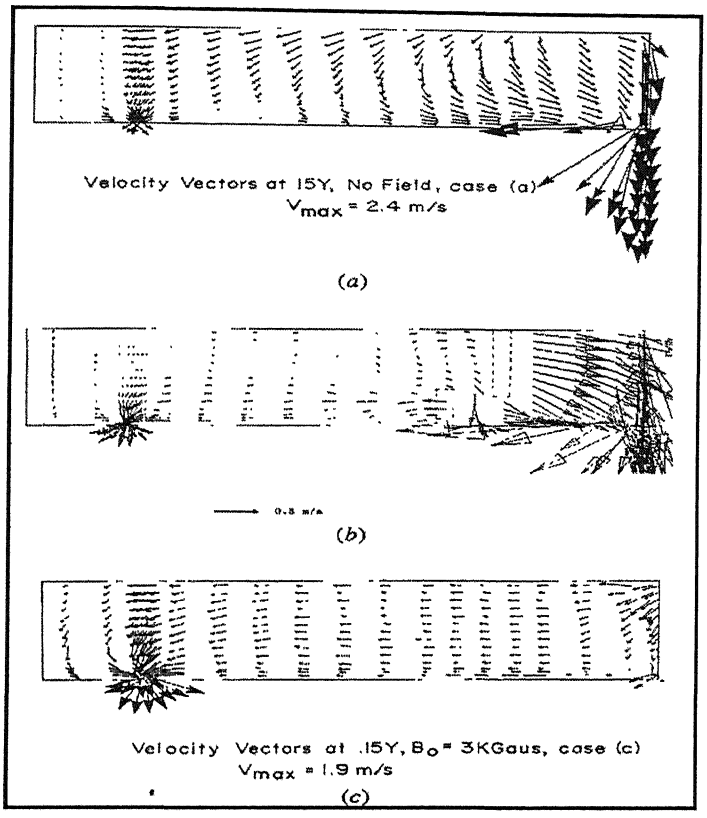

Figure 1.9 (a, b and c): Computed velocity field at the central vertical plane with (a) no flow control devices, (b) with a dam and a weir insert and (c) Magnetic field imposed on the system in horizontal direction

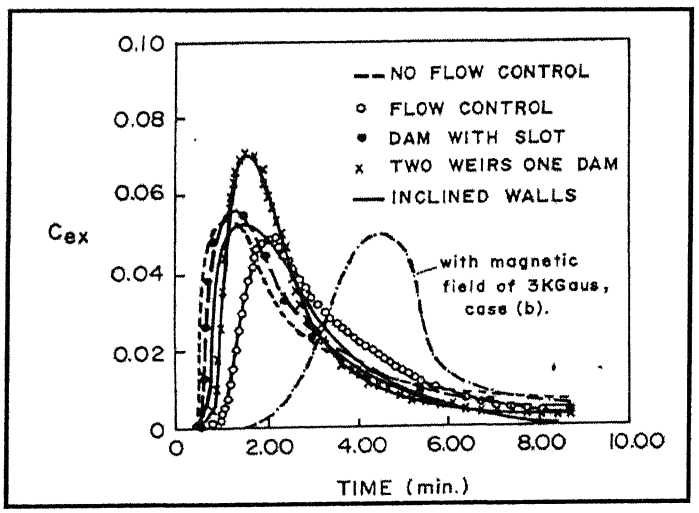

Figure 1.10: Tracer dispersion curve for all configurations

1.3 DESCRIPTION OF THE FLUENT

1.3.1 List of Commercial Packages

The key developments in the mathematical modeling are the introduction of computers. As we know that the mathematical modeling often involves solving the partial differential equations together with a given set of boundary conditions; the use of computers come into play as the equations are often nonlinear (requires iterative solution methodology) and hence arriving at realistic solution is often time intensive. The remarkable speed of digital computers can minimize the severity of computational efforts significantly.

The numerical solution of mathematical model equations relevant to transport phenomena in steelmaking is carried out via computer programs developed in-house or via readily available software packages like PHEONICS, FLUENT etc. The former can be used for representing a single, relatively simple problem .On the other hand, for far too complex problems, the commercial software packages can be used and results obtained in a reasonable time frame together with elegant post processing. The list of available software package is given in the Table 1.3 [3]. These software packages are mainly written the basic programming languages like C, C++ and FORTRAN which uses graphics interfaces to give the information in a meaningful way. These packages are available to do thermodynamic equilibrium calculations, solve heat flow and fluid flow problems, solve heat conduction and thermal stress problems, and even tackle problems with free boundaries. Softwares are available to perform complex solid mechanics problems as well. The software packages are user friendly and offer considerable user flexibility for simulating a real engineering problem.

Name	Application	Method
ANSYS	Structural, thermal, electrical, magnetic	Finite element
ABAQUS	Structural, thermal, electrical, magnetic	Finite element
NASTRAN	Structural	Finite element
FIDAP	Fluid dynamics	Finite element
PHEONICS	Fluid dynamics, heat transfer, chemical reaction	Finite volume
FLOW 3-D	Fluid dynamics	Finite difference
FLUENT	Fluid dynamics, heat transfer	Finite volume
NEKTON	Fluid dynamics, heat transfer	Finite element (spectral)
NISA	Fluid dynamics, heat transfer	Finite difference
IMSL	Math/statistical library	
LINPACK	Math library	
MINPACK	Minimization/optimization library	
EISPACK	Eigenvalue library	
ASPEN	Flowsheet simulation	Sequential modular
FLOWTRAN	Flowsheet simulation	
SOLGASMIX	Chemical equilibrium	
ECES	Aqueous chemistry	
F*A*C*T	Phase diagrams, chemical equilibrium	
ROMULUS	Solids modeling	
PATRAN	Solids modeling, finite element pre and post processing	
SLAM II	Event simulation	
MAGNUM	Magnetics	Finite element

Table 1.3: Partial list of available software for the CFD analysis

In the following sections, a brief description on the CFD package FLUENT which has been extensively applied in the present work is provided.

1.3.2 Salient features of FLUENT

The FLUENT [21] is a state-of-the-art computer program for modeling fluid flow and heat transfer in complex geometries. FLUENT provides complete mesh flexibility, solving the flow problems with unstructured meshes that can be generated about complex geometries with relative ease. FLUENT is written in the C computer language and makes full use of the flexibility and power offered by the language. It uses the Finite volume scheme of discretization. Consequently, true dynamic memory allocation, efficient data structures, and flexible solver control are all made possible. In addition, FLUENT uses a client/server architecture, which allows it to run as separate simultaneous processes on client desktop workstations and powerful compute servers, for efficient execution, interactive control, and complete flexibility of machine or operating system type. All functions required to compute a solution and display the results are accessible in FLUENT through an interactive, menu-driven interface. The user interface is written in a language called Scheme, a dialect of LISP. The advanced user can customize and enhance the interface by writing menu macros and functions.

The FLUENT package includes the following products:

1. FLUENT, the solver.
2. prePDF, the preprocessor for modeling non-premixed combustion in FLUENT.
3. GAMBIT, the preprocessor for geometry modeling and mesh generation.
4. TGrid, an additional preprocessor that can generate volume meshes from existing boundary meshes.
5. Filters (translators) to import surface and volume meshes from CAD/CAE packages such as ANSYS, CGNS, I-DEAS, NASTRAN, PATRAN, and others.

Figure 1.11 shows the organizational structure of these components.

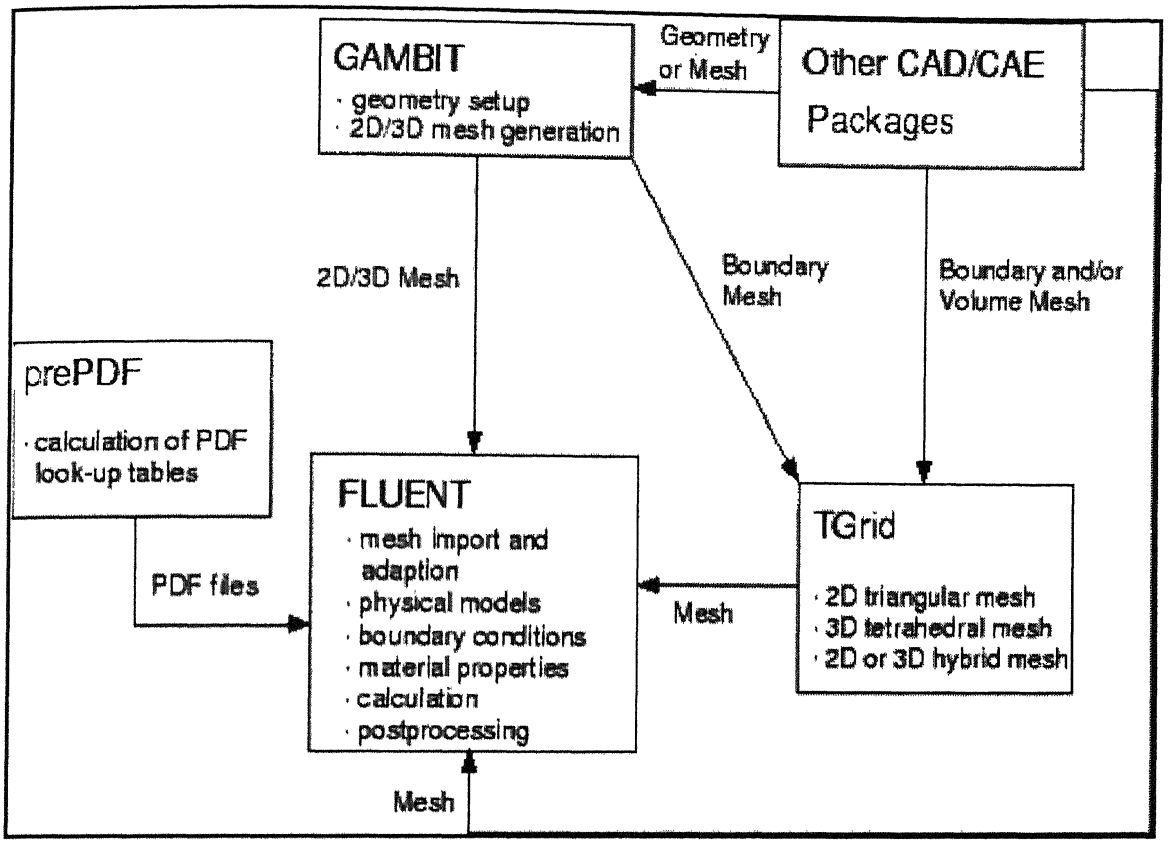

Figure 1.11: Basic program structure for FLUENT

One can create geometry and grid using GAMBIT and use TGrid to generate a triangular, tetrahedral or hybrid volume mesh from an existing boundary mesh (created by GAMBIT or a CAD/CAE package). It is also possible to create grids for FLUENT using ANSYS, CGNS, I-DEAS, PATRAN, NASTRAN. Once a grid has been read into FLUENT, all remaining operations are performed within the solver. These include setting boundary conditions, defining fluid properties, executing the solution, refining the grid, and viewing and post processing the results. FLUENT uses unstructured meshes in order to reduce the amount of time spent on generating meshes, simplifies the geometry modeling and mesh generation process, model more-complex geometries than one can handle with conventional, multi-block structured meshes, and let the user adapt the mesh to resolve the flow-field features. FLUENT can also use body-fitted, block-structured meshes. FLUENT is capable of handling triangular and quadrilateral elements (or a combination of the two) in 2D, and tetrahedral, hexahedral, pyramid, and wedge elements

(or a combination of these) in 3D. This flexibility allows the user to pick mesh topologies that are best suited for your particular application.

The FLUENT software has the following modeling capabilities:

1. 2D planar, 2D axisymmetric, 2D axisymmetric with swirl (rotationally symmetric), and 3D flows.
2. Quadrilateral, triangular, hexahedral (brick), tetrahedral, prism (wedge), pyramid, and mixed element meshes.
3. Steady-state or transient flows.
4. Incompressible or compressible flows, including all speed regimes (low subsonic, transonic, supersonic, and hypersonic flows).
5. Inviscid, laminar, and turbulent flows.
6. Newtonian or non-Newtonian flows.
7. Heat transfer, including forced, natural, and mixed convection, conjugate (solid/fluid) heat transfer, and radiation.
8. Chemical species mixing and reaction, including homogeneous and heterogeneous combustion models and surface deposition/reaction models.
9. Free surface and multiphase models for gas-liquid, gas-solid, and liquid-solid flows.
10. Lagrangian trajectory calculation for dispersed phase (particles/droplets/bubbles), including coupling with continuous phase.
11. Cavitation model.
12. Phase change model for melting/solidification applications.
13. Porous media with non-isotropic permeability, inertial resistance, solid heat conduction, and porous-face pressure jump conditions.
14. Lumped parameter models for fans, pumps, radiators, and heat exchangers.
15. Inertial (stationary) or non-inertial (rotating or accelerating) reference frames.
16. Multiple reference frame (MRF) and sliding mesh options for modeling multiple moving frames.

17. Mixing-plane model for modeling rotor-stator interactions, torque converters, and similar turbomachinery applications with options for mass conservation and swirl conservation.
18. Dynamic mesh model for modeling domains with moving and deforming mesh.
19. Volumetric sources of mass, momentum, heat, and chemical species.
20. Material property database.
21. Extensive customization capability via user-defined functions.
22. Dynamic coupling with GT-Power and WAVE.
23. Acoustics module.
24. Magnetohydrodynamics (MHD) module.
25. Continuous fiber module.

The capability and flexibility that FLUENT has, find application in numerous areas. Some of the applications of the FLUENT include the following:

1. Process and process equipment applications
2. Power generation and oil/gas and environment applications
3. Aerospace and turbomachinery applications
4. Automotive applications
5. Water management applications
6. Marine applications
7. Electronics and HVAC appliances
8. Materials processing applications
9. Architectural design and fire research

1.3.3 GAMBIT

Geometry And Mesh Building Interactive Tool (GAMBIT) [22] is the pre processor for the FLUENT software in which the graphic details is made. The GAMBIT consists of a graphics window panel in which several options for creating and meshing of the geometries are given. It is commonly called as Graphical User Interface (GUI). Within the GUI, there are eight components present. They are

1. Graphics window
2. Main menu bar
3. Operation tool pad
4. Form field
5. Global Control tool pad
6. Description window
7. Transcript window
8. Command text box

The graphics window is the region of the GUI in which the model is displayed. It is split into four quadrants which show the models in different views. The main menu bar consists of file, edit, solver and help. The operations performed by these items are given in Table 1.4.

Menu Item	Operations
File	Create, open, and save GAMBIT sessions; print graphics; edit and run journal files; clean up journal files; import and export model data; exit the program
Edit	Edit session titles; launch a text editor; edit model parameters and program defaults
Solver	Specify a computational solver – ANSYS, FLUENT4,FLUENT5/6
Help	Launch the local web browser and open the GAMBIT online help document

Table 1.4: Operations performed by the main menu bar items in GAMBIT

The operation tool pad consists of a field of command buttons, each of which performs a specific function associated with the process of creating and meshing a model. Within the operation tool pad, command buttons are grouped according to their hierarchy and purpose in the overall scheme of creating and meshing the model. The topmost group constitutes the main pad. All other command button groups constitute sub pads. The main pad includes Geometry – create and refine model geometry, Mesh - create and refine the mesh, Zone - Specify boundary and continuum zone types and Tools - specify coordinate systems and grids and perform specialized GAMBIT operations. The sub pad command

buttons perform operations related to the overall purpose of the main pad. The geometry and mesh pads consist of sub pads of creating and meshing of vertices, edges, faces and volumes. The zone pad has sub pads of boundary type and continuum.

The form field is opened by clicking any of the sub pads. This allows specifying parameters related to modeling and meshing operations, the assignment of boundary attributes, and the creation and manipulation of GAMBIT coordinate systems and grids. Specification forms can be used, for example, to define the radius of a sphere, designate edges of the model to be aligned, or select a particular meshing option from a list of available procedures. The global tool pad is to allow the user to control the layout and operation of the graphics window, specify the appearance of the model as displayed in any particular quadrant, and undo GAMBIT operations. The purpose of the Description window is to display messages describing the various GUI components, including sashes, fields, windows, and command buttons. The purpose of the transcript window is to display a log of commands executed and messages displayed by GAMBIT during the current modeling session. The Command text box allows the user to perform GAMBIT modeling and meshing operations by means of direct keyboard input, rather than by means of mouse operations on the GUI.

The geometry is created by the geometry option in the operation tool pad by creating vertex, line, face and volume. The better way to draw a complex geometry is starting from vertex. If the geometry is simple, the ready made options can be used which are available in the GAMBIT. The created geometry (vertex, line, face and volume) can be moved and/or copied by move/copy option which is present in all stages. The Boolean operations also can be performed for the geometry. Once the geometry is created, the next operation is meshing.

The meshing types are boundary layer, edge, face and volume. The cases which are boundary layer sensitive should use the boundary layer meshing. The geometry is first meshed along the edges, then faces and at the last volumes is meshed. There are different

types of meshing schemes available for the face and volume meshing. They are listed in Table 1.5.

Mesh	Elements	Type
Face	Quadrilateral	Map
		Sub Map
		Pave
		Triangle primitive
	Triangle	Pave
	Quadrilateral/Triangle	Map
		Pave
		Wedge Primitive
Volume	Hexagonal	Map
		Sub Map
		Tetragonal Primitive
		Cooper
		Stair step
	Hexagonal/wedge	Cooper
	Tetragonal/Hybrid	TGrid

Table 1.5: Mesh schemes available in GAMBIT

For the simple geometries, the quadrilateral or triangle meshing are used. For complex geometries and multi phase problems, hexagonal scheme is generally used. The tetragonal/hybrid – tgrid mesh scheme is used in the present study. The mesh spacing is given either by interval size, interval count or percentage of shortest edge. After meshing, the specification of boundary condition should be done. Before that the solver panel should be reset to the specific solver (in the study FLUENT 5/6). The desired boundary conditions are set for each faces in 3D geometry and edges in 2D geometry. The

continum type is set for the geometry after the boundary conditions are specified. Finally, the file is saved and exported in the form of mesh file (.msh) to the FLUENT.

1.3.4 FLUENT

The numerical simulation for the geometry created in GAMBIT is done in the FLUENT solver. The general steps for the FLUENT [21] simulation are given below.

1. Start the appropriate solver for 2D or 3D modeling.
2. Import the grid.
3. Check the grid.
4. Select the solver formulation.
5. Choose the basic equations to be solved: laminar or turbulent (or inviscid), chemical species or reaction, heat transfer models, etc. Identify additional models needed: fans, heat exchangers, porous media, etc.
6. Specify material properties.
7. Specify the boundary conditions.
8. Adjust the solution control parameters.
9. Initialize the flow field.
10. Calculate a solution.
11. Examine the results.
12. Save the results.
13. If necessary, refine the grid or consider revisions of the numerical or physical model.

The overview of the FLUENT menu is given in Table 1.6. The solver is usually being 2D or 3D which represents the single precision solver. The double precision solver (2DDP or 3DDP) is also available which are used in case of geometry features having disparate length scale, geometry involve multiple enclosures via small diameter pipes and/or for conjugate problems involving high thermal conductivity ratios or high aspect ratio grids.

Solution Step	Menu
Import the grid.	File menu
Check the grid.	Grid menu
Select the solver formulation.	Define menu
Choose basic equations.	Define menu
Material properties.	Define menu
Boundary conditions.	Define menu
Adjust solution controls.	Solve menu
Initialize the flow field.	Solve menu
Calculate a solution.	Solve menu
Examine the results.	Display menu
	Plot menu
	Report menu

Table 1.6: Overview of FLUENT menus

The mesh file is imported from the GAMBIT through FILE→READ→CASE→filename (*.msh). Once the mesh file is read, the file is checked for grid through GRID→CHECK. This step is necessary so that any defect during meshing or an incomplete meshing can be identified. Then the appropriate solver is selected from DEFINE→MODELS→SOLVER. The default settings are segregated, 3D, steady state, absolute and implicit. The user can modify the solver according to the problem. The other specifications such as viscosity prescription, thermal energy model, multiphase, species transport, discrete phase, solidification and melting, acoustics and pollutants are selected according of the problem. In the present study, SOLVER and viscous models (laminar flow conditions) are selected as default. After selecting the model, the materials are specified in the DEFINE→MATEIALS panel. The user can change and create the materials in that panel. The next step is to define operating conditions in DEFINE→OPERATING CONDITIONS where the specification of operating pressure is made. Then the boundary conditions are specified in DEFINE→BOUNDARY CONDITIONS. The boundaries are specified with values such as velocity in velocity inlet, heat flux on walls etc. The next step is to specify the solution controls from SOLVE→CONTROLS→SOLUTION. Here the change of under relaxation

parameters and change of solution methodology are prescribed. In the study, default conditions are used. The pressure – velocity coupling is done by SIMPLE method and momentum equations are solved by first order upwind method. Then the solution is initialized by SOLVE→INITIALIZE→INITIALIZE. The initial values for pressure and x, y and z velocity are taken as zero. The residuals are monitored from SOLVE→MONITOR→RESIDUALS. The iterations are initiated from SOLVE→ITERATE. The number of iterations depends on the grid size and geometry. Typically a large number of iteration is specified. The problem is terminated once convergence is reached. The default convergence criteria of 10^{-3} were applied on all variables.

After convergence, the post processing is done. The contours of the velocity, pressure, shear stress etc are seen from DISPLAY menu. The results are obtained from REPORT menu from which surface integrals, volume integrals, fluxes, forces etc of the properties can be obtained for a specified area in the calculation domain. At last, the files are saved as a case and data file invoking WRITE→CASE AND DATA. The FLUENT software is widely used in steelmaking industry to study the flow phenomena. In this section, some of the modelling examples are discussed briefly.

Secondary steelmaking has become an important, integral processing route for the production of quality steel. The final steel chemistry and casting temperature from a Basic Oxygen Furnace (BOF) or Electric Arc Furnace (EAF) is adjusted by secondary steel making or secondary metallurgy route for adequate process performance. As the liquid steel is tapped from the furnace, tap-time additions and heat loss create a highly dynamic thermo-physical process in the liquid bath. During the subsequent holding period, the liquid layers in the ladle undergo thermal stratification resulting from natural convection. Thermal stratification is detrimental to quality casting. Tap temperature, holding time, ladle preheat and ladle life significantly influence the rate of such thermal stratification. Argon gas purging through the liquid steel bath helps to generate enough bath turbulence to cause rapid thermal homogenization. Stirring with argon also enhances the mixing rate for chemical additions. Using Fluent various processes in secondary steel

making can be analyzed and optimum process parameters established. For example, effect of purging rate Vs. Heat size, effect of ladle preheat, effects of carry-over slag and synthetic slag volume, thermal effects and mixing rates of various chemical additions all can be efficiently modelled via FLUENT. As a typical capability of FLUENT, Figure 1.12 shows the temperature field of the ladles with and without Argon purging. The first image here shows the growth of thermal stratification in a 130-ton steel ladle after 20 minutes of holding. The thermally stratified bath is then agitated by purging of argon gas from the bottom and as the second image shows little or no stratification after about 3 minutes of argon purging [5].

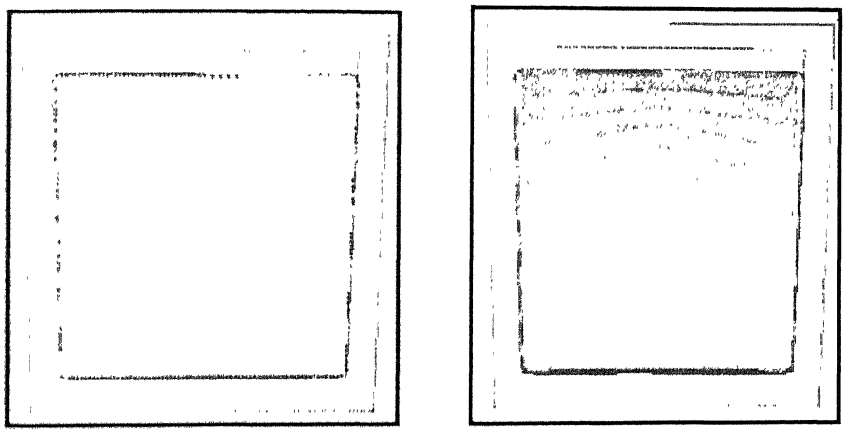

(a) (b)

Figure 1.12 (a and b): Temperature field in ladles with and without Argon purging

Oxygen steel making is by far the most popular steel making process. As is well known that energy efficiency of steel making largely depends on the tap temperature, the ladle preheat and the steps followed in the secondary steel making processes. The pig iron in the vessel is decarburized by the high-speed, strong, flow of oxygen through the lance at high operating temperature. The blowing process, equipment and ancillaries can be analyzed using CFD. Furthermore, CFD can also be used to optimize various parameters (e.g., blowing sequence, flow rate, pressure and bath-temperature) depending on heat size, scrap volume, vessel-life, hot metal temperature, and lance condition. Almost all BOF auxiliaries (de-dusters, hoods, gas supply, blowers, pumps and various ductings) are routinely analyzed using CFD. Fume extraction and de-dusting of the BOF

flue can also be improved upon with CFD based analyses [5]. Understanding the basic mixing pattern and flow in the vessel can also be accomplished through CFD. Figure 1.13 shows the potential of CFD in which, velocity field at lance tip and instantaneous distribution of steel and gas phases within the vessel is shown.

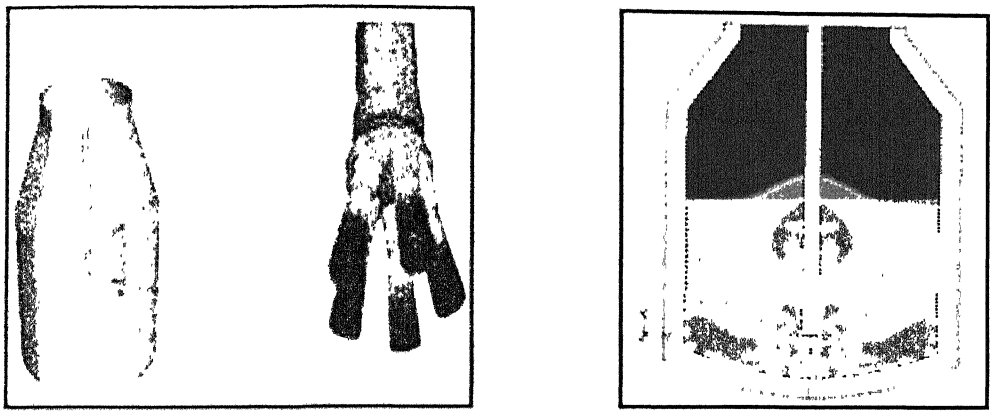

(a) (b)

Figure 1.13 (a and b): velocity field at lance tip and instantaneous distribution of steel phase during oxygen blowing in a BOF

The tundish is a buffer for liquid steel during the continuous casting of steel. There is another important aspect of the tundish operation - the need to cast different grades of steel sequentially through the same caster. The tundish allows changing of the ladle (and hence of the steel grade) but there is an unavoidable mixing of two different grades of steel in the tundish. This produces cast slabs of intermixed grades that are difficult to classify. Keeping the intermixed grade volume to a minimum is a plant target. CFD is used to estimate the grade change over time for a particular tundish. Flow distribution in the tundish has very critical influence on the casting process in terms of quality, productivity and economics. Use of CFD is becoming increasingly popular in designing and optimizing tundish furnitures (weirs, dams, and baffles) [5]. It is also possible to study the effects of various process parameters and practices and thereby optimize the process to achieve the minimum amount of intermixed grade steel. Concentration contours in a continuous casting tundish during the grade change operation

is shown in Figure 1.14. Red was the old grade that is almost replaced, by the intermediate grades and blue is the new grade.

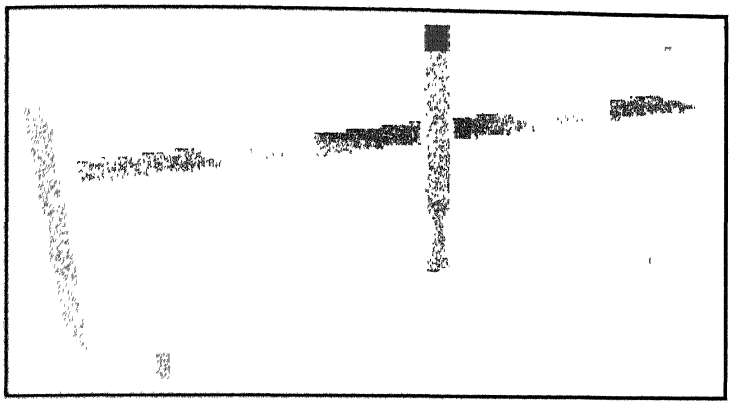

Figure 1.14: Concentration contours in a tundish during the grade transition

Continuous casting of steel is the predominant means of producing steel slabs, billets, blooms and rods. The process involves a wide range of operational parameters, such as steel grade, required and available superheats, casting speed and cross-section, presence of any electro-magnetic stirring (EMS), mold-water temperature, flow-rate and distribution, and the effectiveness of spray cooling zone. Because this wide set of important process parameters interacts in a non-linear manner, process control is highly susceptible to instabilities, leading to various defects and sometimes even breakout. CFD is very effectively used to study the mold flow, solidification, mush formation, design of submerged entry nozzle (SEN), analysis of mold powder performance, effects of turbulence, EMS, argon purging around the SEN and EMS. Figure 2.5 shows the results generated via CFD illustrating the difference in flow field with an existing as well as modified SEN design at NKK steel, Tokyo [5]. There are many other examples cited within the literature which appear to indicate that Fluent has been applied by numerous investigators to investigate the process dynamics of steelmaking.

Other examples where the FLUENT is used in the steelmaking industry are: Fume extraction in BOF and EAF, Dust catcher in Electrostatic filter, Recirculating flow in Vacuum degasser, Burner design etc.

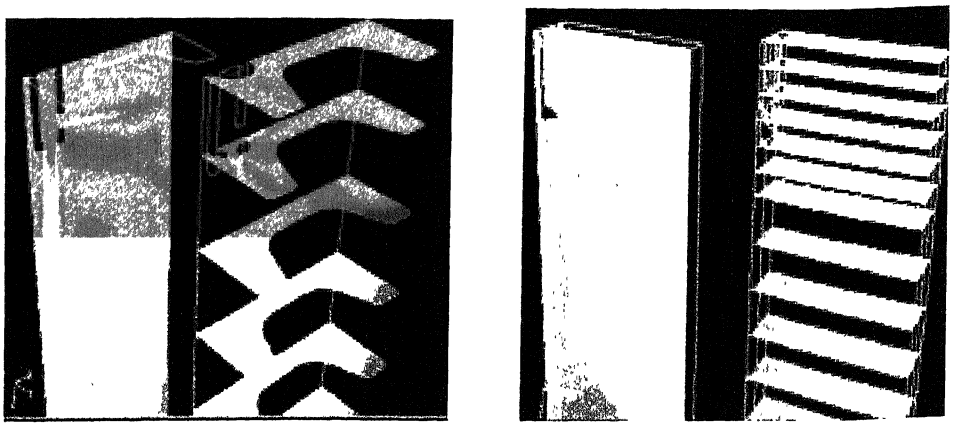

(a) (b)

Figure 1.15 (a and b): Flow field at SEN – (a) As it is and (b) With modified design

1.4 SCOPE OF THE WORK

The use of Computational Fluid Dynamics in the field of steelmaking has given the opportunity to have detailed knowledge about the process taking place in steelmaking vessels, ladles, tundishes and continuous casting moulds etc. These give us opportunity to study the processes effectively and also optimization of the processes leading to higher productivity. The use of CFD has become more common now-a-days for predicting rate phenomena in materials processing for various reasons mentioned already.

The main aim of the present work is to study the fluid flow phenomena in rotating viscometers with the aid of a commercial CFD software FLUENT, investigate the design of such viscometers computationally and to validate FLUENT based model through comparison of predicted and experimental torque values reported in the literature. The present work is expected to set the ground work for carrying out more elaborate numerical calculations for complex steelmaking systems via the FLUENT which is now available in our main frame computer. Apart from this, the present work is aimed to address and assess the currently used approaches for viscosity measurements in rotating viscometers through detailed numerical simulation, which has not been reported in the literature till date.

1.5 LAYOUT OF THE THESIS

The body of the thesis consists mainly of four chapters. Chapter one presents a brief introduction to modeling, literature review and relevance of CFD in steelmaking. This chapter also provides a description of the commercial CFD package FLUENT. In chapter two, description of the problems dealt, numerical simulation together with results and discussion are presented for two different viscometer configurations. Chapter three presents the conclusions derived from the present work. The thesis ends with the suggestions and recommendations for the future work in chapter five.

FLUID FLOW MODELLING IN ROTATING VISCOMETERS

2.1 PROBLEM 1 –MEASUREMENT OF VISCOSITY OF $CaO-MgO-Al_2O_3-SiO_2$ MELT IN A ROTATING VISCOMETER

2.1.1 Problem Description

An important mechanical property of fluids is *viscosity. Viscosity* is defined as the internal friction of a fluid. Physical systems and applications as diverse as fluid flow in pipes, the flow of blood, flow of molten metals and slags, lubrication of engine parts, the dynamics of raindrops, volcanic eruptions, planetary and stellar magnetic field generation, etc, all involve fluid flow and are controlled to some degree by fluid's viscosity. From the Newton's law of viscosity [23], the shear stress (τ), the velocity gradient and the viscosity (μ) are related in the context of parallel flows as:

$$\tau_{yx} = -\mu \frac{dv_x}{dy} \tag{2.1}$$

The importance of viscosity in metallurgy is readily evident since viscosity of slags and metals constitute important kinetic data and therefore, are naturally of considerable importance (i.e., to the modelling and controlling of various metallurgical processes). Naturally, therefore, significant efforts have been made by researchers to measure viscosity of a diverse range of metallurgical melts [24-31]. In practically all these investigations, a rotating viscometer, either with a rotating crucible [31] or a rotating cylinder or spindle [24-30] has been applied. A typical measurement, for example, involves imparting a rotational motion to either the crucible or the spindle and

recording the corresponding the equilibrium torque experienced by the cylinder or spindle i.e., the entire submerged assembly. From the measured torque, melt viscosity is deduced following one of the two popular approaches, and these include

- A technique relying entirely on calibration [24], in which a torque vs. viscosity relationship established a *priori* from standard melts, is applied to translate the measured torque into viscosity.
- A simplified one dimensional momentum transfer analysis wherein, wall shear stress inferred from the measured torque is equated against the corresponding shear strain rate and thereby, melt viscosity is determined [30].

According to the simplified theory of flows in rotating viscometers [23,30], the viscosity of the liquid or melt is obtained by dividing the shear stress with the corresponding shear strain rate, both evaluated at the spindle surface,

$$\mu = \left[\frac{\tau}{\theta}\right]_{R=R_{spindle}} \tag{2.2}$$

In Equation (2.2), θ and τ are the shear strain rate (s^{-1}) and shear stress (Pa) at the spindle surface and are respectively given by [23,30]:

$$\theta = \frac{2}{1-\frac{R_{spindle}^{\ 2}}{R_{crucible}^2}}\left(\frac{2\pi}{60}\right)\dot{n} \tag{2.3}$$

and

$$\tau = \frac{Q}{2\pi R_{spindle}^2 L_{spindle}} \tag{2.4}$$

Where,

Q = torque in Nm.

$R_{spindle}$ = radius of spindle in m.

$L_{spindle}$ = length of spindle in m.

$\dot{n}$ = speed of rotation in rpm.

It can be readily seen from the above that the certainty with which melt viscosity is estimated from Equation (2.2) depends in turn on the accuracy with which the measured torque is translated to a surface shear stress value via Equation (2.4). Since neither the torque ~ shear stress relationship nor the expression for shear strain rate given above are applicable to the viscometer geometry in a rigorous sense, consequently, a sufficiently accurate value of shear stress is unlikely to result from the uni-dimensional flow theory (viz., on the basis of Equation (2.2) – (2.4)) considering the surface area of the spindle alone (as in Equation (2.4)). This is so as the associated end effects as well as the additional resistance to the flow offered by the shaft attached to the rotating spindle are not taken into account in the uni-dimensional mathematical treatment. Needless to mention, such effects are required to be accommodated in the overall hydrodynamic analysis, if shear stress and hence melt viscosity are to be deduced from the measured torque with any certainty. This is achieved by embodying an effective value of the denominator in Equation (2.4), inverse of which is often referred to as viscometer cell parameter and denoted as C_s [30]. Typically, by calibrating the viscometer against melts/liquids of known viscosity, an effective and reasonably accurate value for the viscometer cell parameter (C_s) is deduced. On the basis of such, shear stresses acting on the rotating assembly can be deduced from the measured torque via. Equation (2.4) fairly accurately, leading to a correct estimate of liquid/melt viscosity.

The foregone discussion implies that uni-dimensional flow theory in conjunction with a set of appropriate calibration data is likely to provide true estimate of shear stress acting on the rotating cylinder and the shaft of the viscometer. Such estimates, as one might anticipate here, would be equivalent to those deduced from a detailed hydrodynamic analysis. Despite numerous studies, there has not been any explicit evidence in the literature to this end. Attempts are yet to be made to directly assess the adequacy of viscosity measurements in rotating viscometers from a fundamental

theoretical stand point. It is therefore naturally important to carry out a detailed hydrodynamic analysis of rotating viscometers and thereby, make an assessment of the procedure [30] applied towards measurements of viscosity in such system.

2.1.2 Case for Simulation

In the present study, the work done by Wright and coworkers [30] on the viscosity measurement of $CaO\text{-}MgO\text{-}Al_2O_3\text{-}SiO_2$ melt with and without spinel particles at a temperature of 1646 K is taken as a case for the simulation. For each specific composition of the melt, these authors measured the torque for various rotational speeds of the spindle in an inner cylinder rotating viscometer. On the basis of such and a properly calibrated C_s value, viscosity of the melt was determined from the uni-dimensional flow theory mentioned already. A schematic diagram of the rotating viscometer together with its principal dimensions is shown in Figure 2.1. Similarly in Figure 2.2, which is reconstructed from reference [30], shows the variation of the measured torque at different rotational speed of the spindle for a $CaO\text{-}MgO\text{-}Al_2O_3\text{-}SiO_2$ melt containing no spinel particles. In the Table 2.1, specific data [30] applied towards reconstruction of Figure 2.2 are given together with the corresponding estimates of shear stress as well as viscosity.

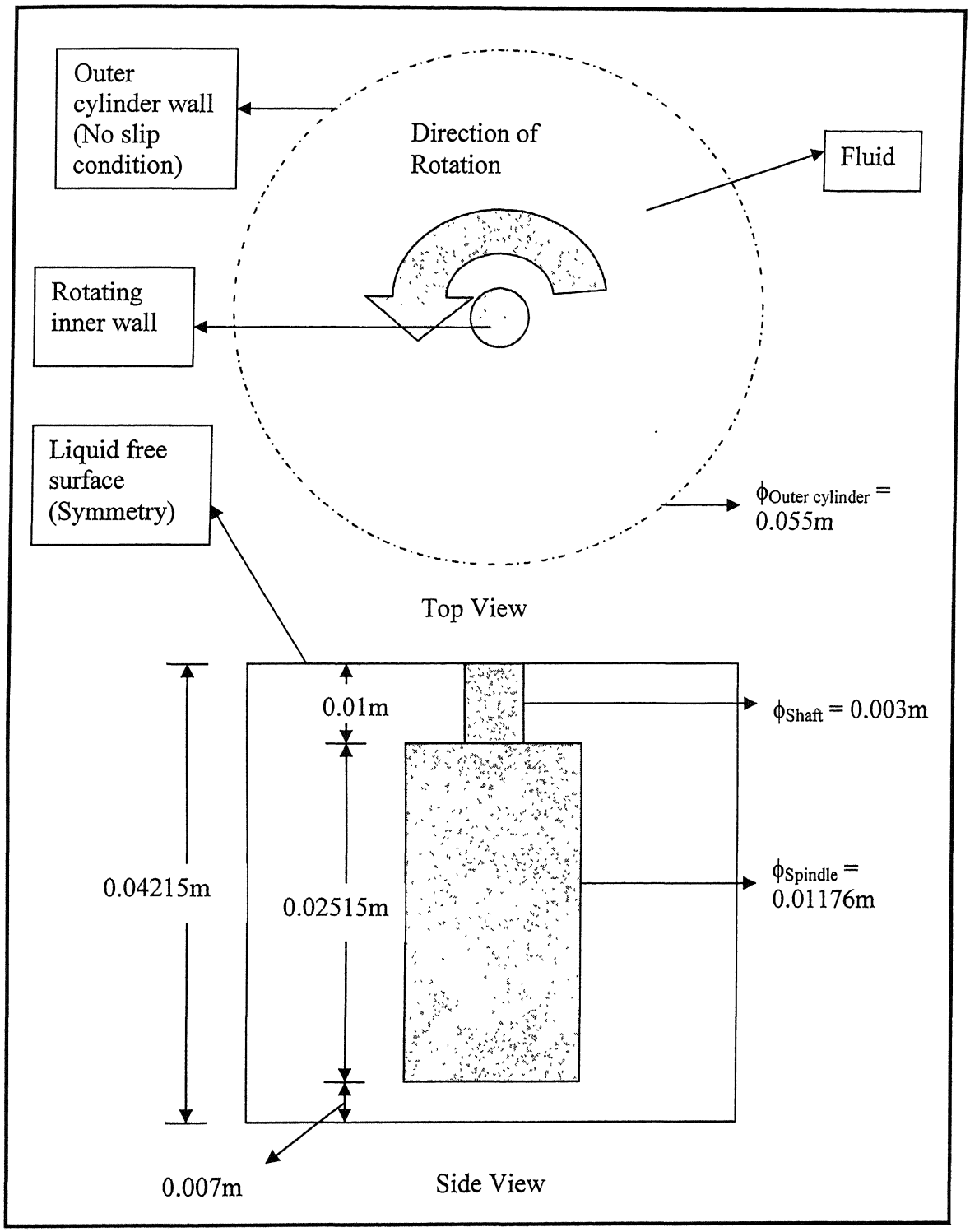

Figure 2.1: Schematic diagram of rotating viscometer with principal dimensions and boundary conditions

Speed, rpm	Torque, N.m.	Viscosity, Pa.s	Estimated shear stress, N/m^2 (=Torque * C_s)
2	8.0844E-06	2.593837	1.1361
2.5	9.4318E-06	2.420915	1.3254
3	1.2127E-05	2.593837	1.7041
4	1.4148E-05	2.269608	1.9881
5	1.7516E-05	2.247992	2.4615
10	3.4359E-05	2.204762	4.8284
12	4.0422E-05	2.161531	5.6805

Table 2.1: Data points reconstructed from the experimental data

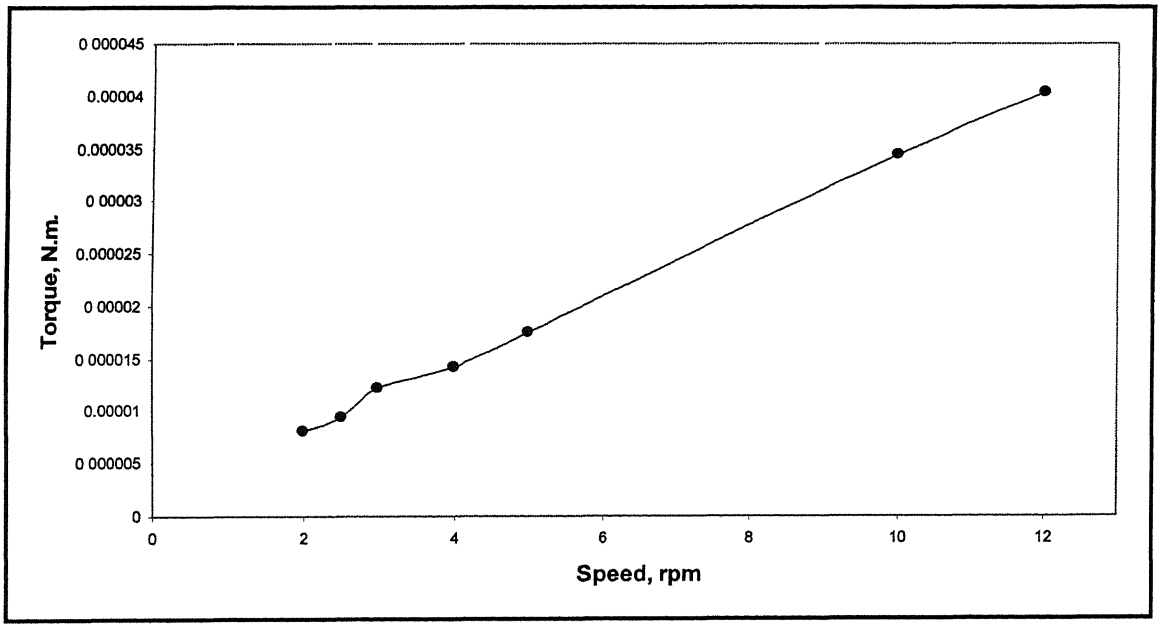

Figure 2.2: Torque vs. Speed curve

There, estimates of shear stress were derived from Equation (2.4) assigning a value [30] of 140530 m^{-3} to the viscometer cell parameter, C_s. Similarly, to deduce melt viscosity, strain rates were directly estimated via Equation (2.3) and applied in conjunction with the estimated shear stress. It is instructive to note here that the average of the estimated melt viscosity corresponds reasonably well to the one (~2.4 Pa.s) suggested by Wright and coworkers [30]. The density of the melt given by the authors is 2650 Kg/m^3.

2.1.3 Model Configuration and Boundary Conditions

Embodying their measured melt viscosity [30] together with the corresponding rotational speed of the shaft – spindle assembly, a mathematical model was developed from first principles to predict fluid flow phenomena in the rotating viscometer geometry, shown in Figure 2.1. The characteristic features of the present formulation are:

- Three dimensional
- Steady state
- Laminar flow
- Isothermal
- Constant viscosity and density

A laminar flow model was considered most appropriate since the ranges of rotational speed of the spindle considered are rather small. The other characteristics of the model are chosen that these conform to the actual experimental conditions of the Wright and coworkers. The boundary conditions applied to the governing flow equations are also shown in the Figure 2.1. There, as seen, symmetry like boundary condition is invoked at the free surface wherein, the normal velocity components as well as gradients of the parallel to surface velocity components are all set to zero. Similarly, the crucible walls are treated as rigid solid walls and a no slip boundary is applied on these. The shaft as well as the spindle of the viscometer are treated like moving boundaries, rotating with a constant angular velocity.

The model equations together with the associated boundary conditions are solved numerically embodying the commercial CFD package FLUENT [21]. As our first step, numerical grid in the computational domain is generated using GAMBIT, embedded in FLUENT. In the numerical solution scheme, a segregated iterative calculation procedure was applied to solve the governing equations of mass continuity and momentum conservation. The SIMPLE algorithm was used to handle the pressure-velocity inter-linkage. A convergence criterion is set to less than 10^{-3} on all variables and computations are carried out until the absolute sum of scaled residuals on the three components of motion and mass continuity all fell below the stipulated value which is shown in Figure

2.3. On the basis of the predicted steady state flow, equilibrium, wall shear stress at the surface of the spindle as well as the shaft of the viscometer are calculated using the "Flux calculation feature" available in the report module of FLUENT6.1. All computation reported in this work are carried out considering a constant melt density.

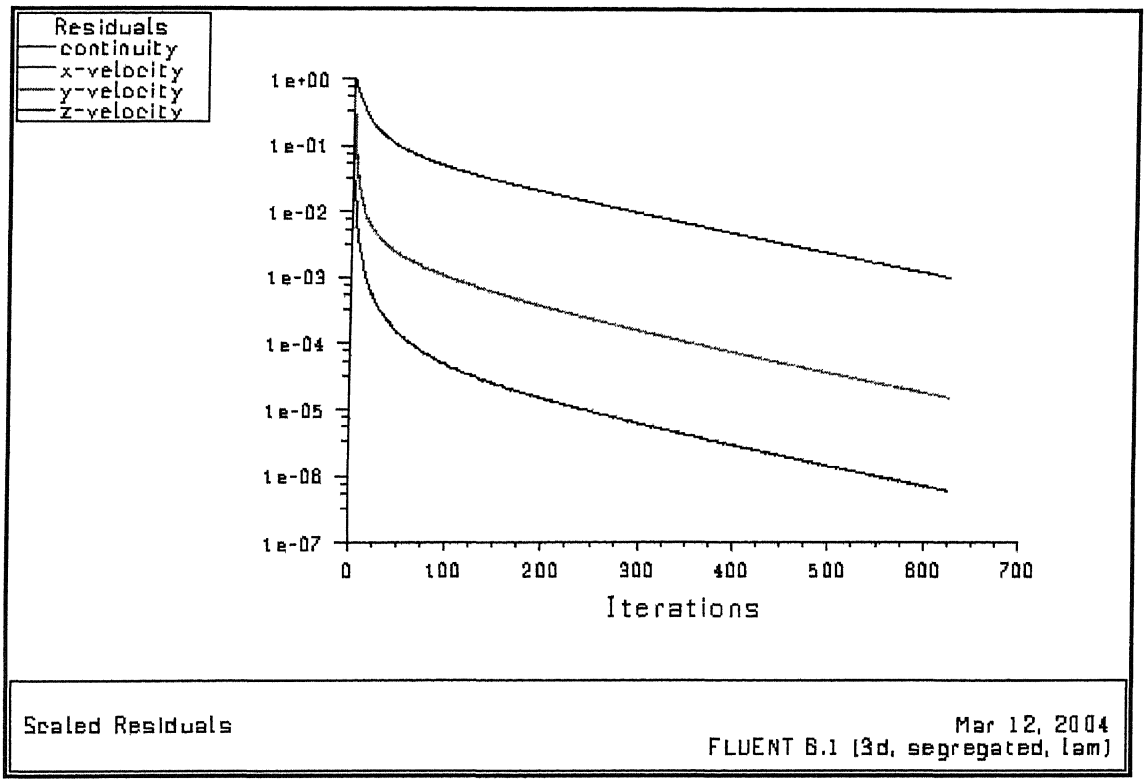

Figure 2.3: Typical convergence curve obtained during flow simulation in flow in viscometer

2.1.4 Comparison of Shear Stress: Estimated vs. Numerical

Approximating the marginally tapered crucible, as a regular cylindrical shaped vessel, numerical computations are carried out for various rotational speeds of the spindle. These then provides the corresponding shear stresses acting on the rotating assembly (shaft + spindle). Direct comparisons between predicted and experimental shear stresses are shown in Table 2.2 and Figure 2.4 for different rotational speeds of the spindle. Excellent agreement between measurement and prediction is readily apparent.

Speed, rpm	Estimated Shear stress, N/m^2	Numerical Shear stress, N/m^2
2	1.1361	1.1378
2.5	1.3254	1.3292
3	1.7041	1.7068
4	1.9881	1.9862
5	2.4615	2.4609
10	4.8284	4.835
12	5.6805	5.6992

Table 2.2: Comparison of shear stresses: Estimated and Numerical

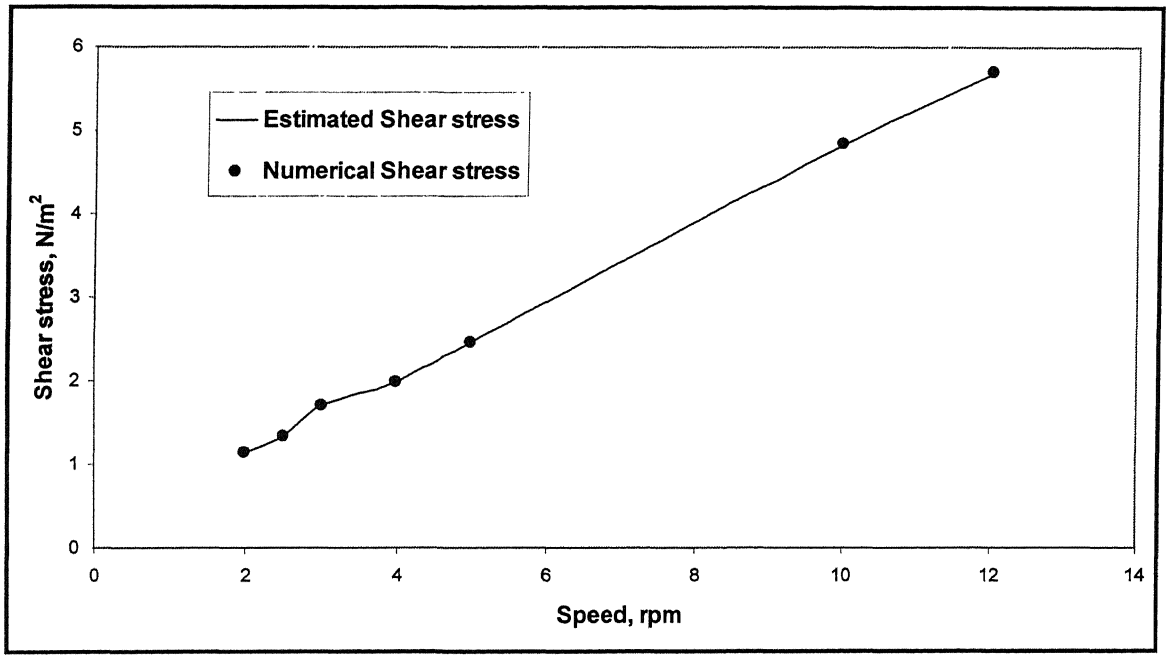

Figure 2.4: Comparison of shear stresses: Estimated and Numerical

Predicted flow pattern on the horizontal plane of the viscometer at a speed of 2 r.p.m. is shown in Figure 2.5. There, relatively high velocity in the vicinity of the rotating spindle surface is readily evident. Furthermore, the rotational flow within the annulus decreases rather sharply with increasing radial distance, thereby creating a near stagnant flow condition in the vicinity of the crucible wall. In comparison to Figure 2.4, the velocity of the melt on the central vertical plane of the viscometer was found to be much weaker ($\sim 10^{-5}$ m/s) by two to three orders of magnitude. Such trends in the computational results are clearly consistent since fluid motion in rotating viscometers is known to be predominantly along the horizontal plane.

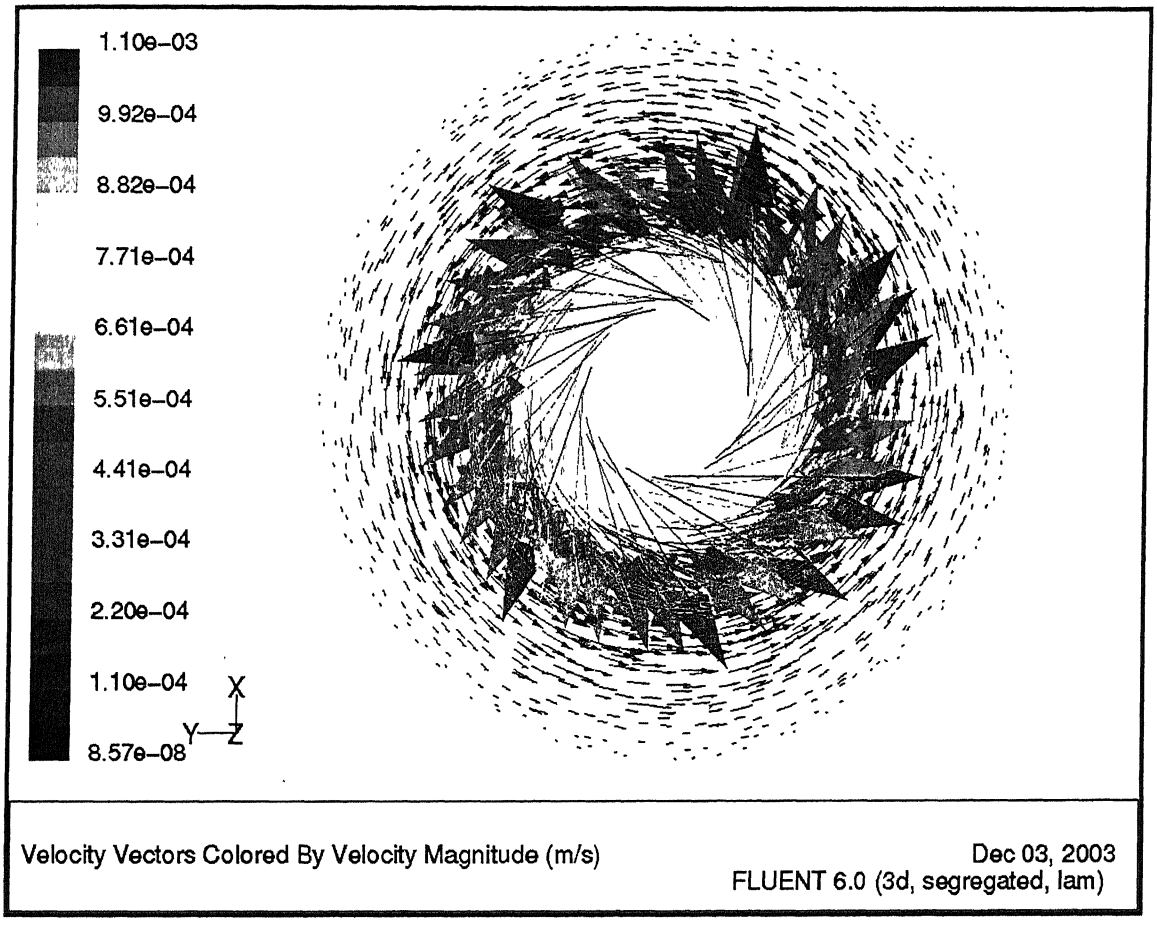

Figure 2.5: Predicted flow pattern on the horizontal plane of the viscometer at a speed of 2 rpm

The Figure 2.6 shows variation of the rotational component of flow along the central vertical plane of the viscometer. From the figure, it is noted that the velocity, v_θ appears to be having a parabolic profile which is consistent with the continuity equation for 1-D flow in cylindrical polar coordinate equation (i.e., $v_\theta \propto 1/r^2$).

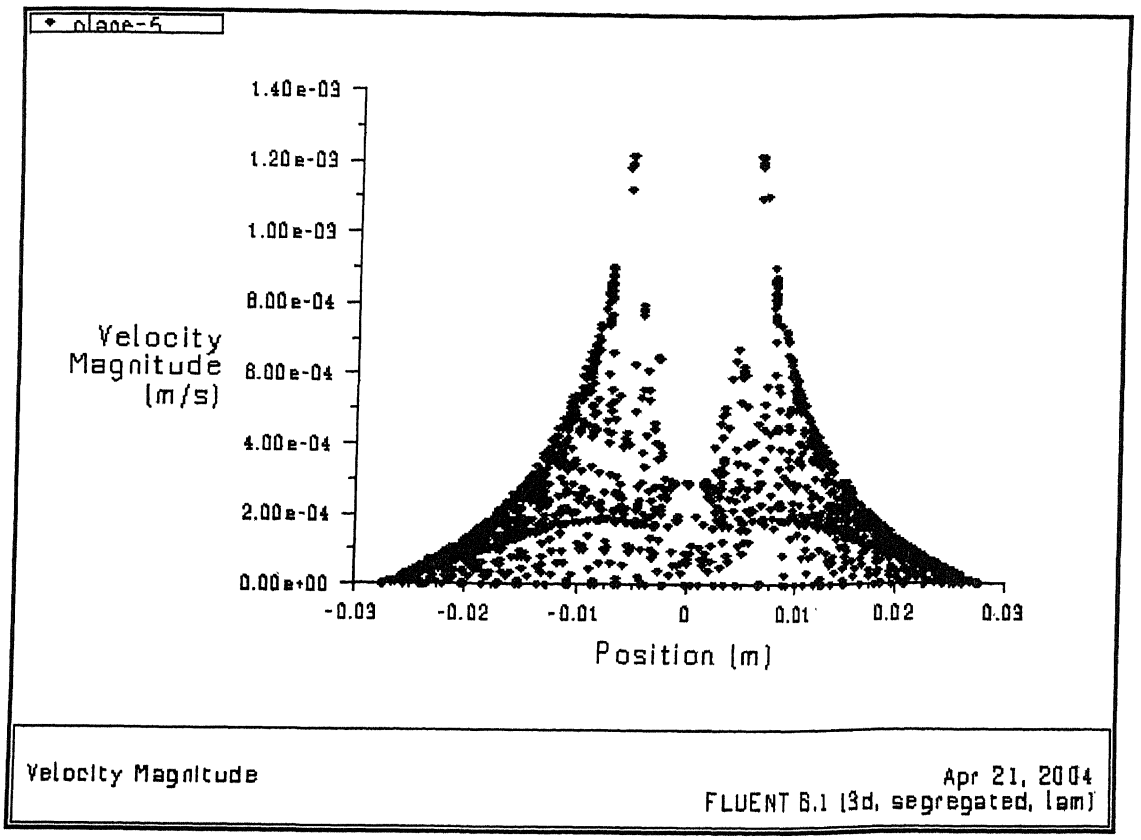

Figure 2.6: Variation of velocity along the central vertical plane of the viscometer

2.1.5 Sensitivity Analysis

2.1.5.1 Tapered vs. Exact cylindrical geometry

Results presented in previous section as pointed out already, were deduced for an idealized situation in which, the taper of the crucible was ignored. Thus to justify the present idealization and to assess the role of crucible taper on the predicted shear stress, FLUENT was adapted to the exact crucible geometry, considering a taper angle 2.7°. Parallel to this, numerical computations were also carried out for various degree of crucible taper such that the latter's role can be better visualized *vis a vis* the design of the viscometer. In Table 2.3, numerically predicted shear stresses for different values of crucible taper are shown together for two extreme speeds with the corresponding experimental measurements. There, it is readily apparent that the taper in the crucible geometry does not influence predicted results to any significant extent. Such trends of

computational results therefore indicate that taper in the crucible geometry is a parameter of secondary importance, as far as the design of such viscometers is concerned.

Speed, rpm	Estimated Shear stress, N/m^2	Numerical Shear stress, N/m^2				
		Without Taper	Taper angle 2.7°	Taper angle 5°	Taper angle 10°	Taper angle 15°
2	1.1361	1.1378	1.1389	1.1391	1.1468	1.1576
12	5.6805	5.6992	5.6981	5.6935	5.7365	5.7905

Table 2.3: Numerical estimates of shear stress for two extreme speeds considering crucible taper

2.1.5.2 Dimension of the Annulus

Shear stresses acting on the surfaces of the rotating assembly were also estimated as a function of the dimension of the annulus. Two extreme speeds of the rotating cylinder were considered for the numerical simulation and the results thus obtained are shown in Table 2.4. The numerical results as one would note here, were derived by keeping the original dimension of the rotating cylinder constant, while varying the diameter of the crucible such that the size of the annular region can be increased or decreased at will. As seen from the Table 2.4, the predicted shear stresses tend to remain practically unaffected as the gap between the rotating cylinder and the crucible is increased beyond the actual design dimension. In contrast, as the annulus is constricted, the predicted shear stress changes. The results appear to indicate that the shear stresses acting on the rotating cylinder would progressively increase as the distance of separation between the crucible and the rotating cylinder is diminished. From the view points of a relatively wide range of smooth viscometer operation as well as reliable reading of the torque data, it is required that the crucible wall exerts negligible influence on the overall hydrodynamics of such systems.

Speed, rpm	Estimated Shear stress, N/m^2	Numerical Shear stress, N/m^2 (c.d. – crucible diameter)			
		Original geometry (c.d. = 0.055m)	50% reduced annular space (c.d. = 0.0334m)	50% enlarged annular space (c.d. = 0.0766m)	100% enlarged annular space (c.d. = 0.0982m)
2	1.1361	1.1378	1.1975	1.1248	1.1201
12	5.6805	5.6992	5.9900	5.6265	5.6033

Table 2.4: Numerically predicted wall shear stress for different crucible diameters at two extreme speeds

Evidently, such objectives can be fulfilled by maintaining an optimum distance of separation between the spindle and the crucible walls. Given such, the results presented so far appear to indicate that a relative diameter ratio of ~5 for the viscometer is appropriate. Interestingly, Figure 2.5 in conjunction with the computational results presented in Table 2.4 suggests that the crucible wall in the given viscometer tends to indeed exert negligible influence on the flow phenomena in the vicinity of the rotating cylinder. Therefore, under such condition, the precise nature of the melt-solid interactions at the stationary crucible wall becomes a subject matter of secondary importance. This is however, not true in situations where the melt wets the spindle or there is slip at the melt-spindle interface. More realistic surface boundary conditions will be required if such situations are to be simulated with any certainty.

2.1.5.3 The influence of the shaft on the predicted shear stress

The shear stress values were also obtained for an idealized situation having only the spindle (i.e., by ignoring the shaft altogether). The result in Table 2.5 shows that the neglecting the shaft tends to have an increased value of the shear stress. This is due to the reduction of surface area of the rotating assembly. This clearly indicates that the shaft's contribution cannot be ignored in the estimation of the melt viscosity correctly.

Speed, rpm	Estimated Shear stress N/m^2	Numerical Shear stress N/m^2	Numerical Shear stress N/m^2 only with spindle
2	1.1361	1.1378	1.1829
2.5	1.3254	1.3292	1.3805
3	1.7041	1.7068	1.7745
4	1.9881	1.9862	2.0706
5	2.4615	2.4609	2.5639
10	4.8284	4.8350	5.0306
12	5.6805	5.6992	5.9183

Table 2.5: Numerical estimates of shear stress considering only the spindle

2.1.5.4 The role of Grid Configurations

Prior to deriving the numerical estimates of shear stress, extensive computational trials were carried out so as to ascertain the influence of nodal configurations on the predicted results. These indicated that solutions tend to become practically grid independent once the spacings between the successive nodal points are limited to about 0.0015 m. This is illustrated in Figure 2.7. Consequently for all numerical simulations reported in the thesis a grid spacing of about 0.0015m was applied.

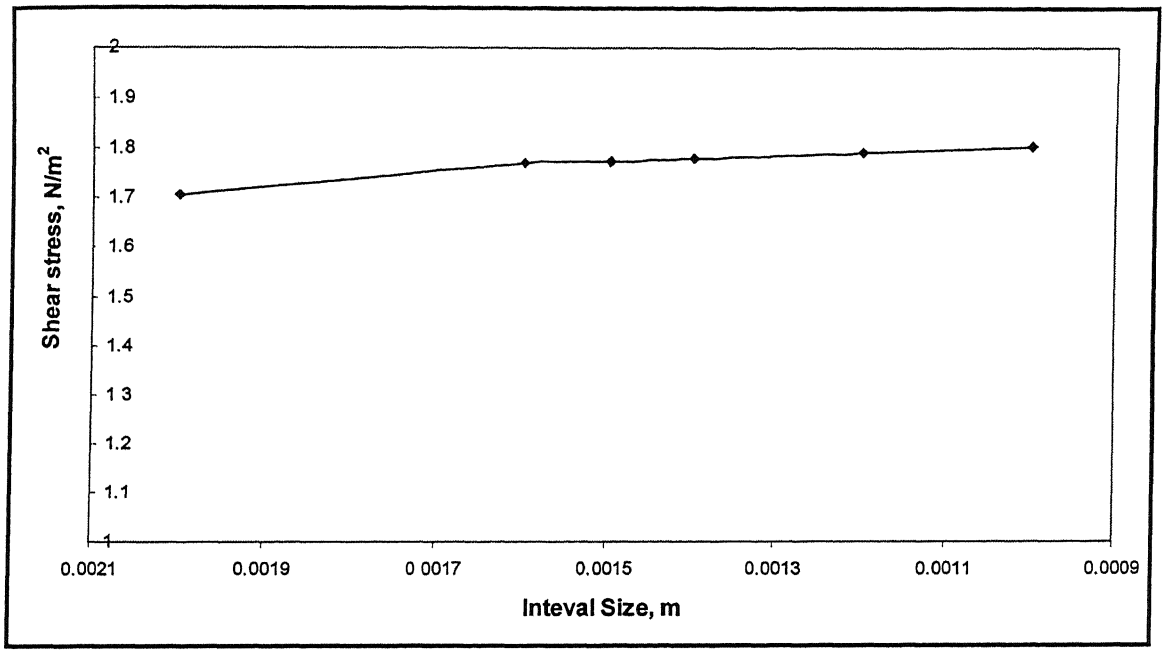

Figure 2.7: Grid independent test curve

2.1.6 Additional Computational Results

2.1.6.1 Contribution of each section of Spindles to shear stress

The various relevant surfaces of the shaft and spindle shown in Figure 2.8. The corresponding computed area fraction shear stresses with their relative percentage contribution are shown for a rotational speed of 2 rpm in Table 2.6. There, it is seen that the shear stress at the spindle's curved accounts for about 84% of the net value. Evidently, end effects are not negligible. On the basis of such, one might therefore anticipate that an accurate estimate of the representative, net wall shear stress from the measured torque is unlikely from the uni-dimensional flow theory considering the dimension of the spindle alone. Given such, the need for the calibration of such viscometers to accommodate end effects etc., become readily apparent.

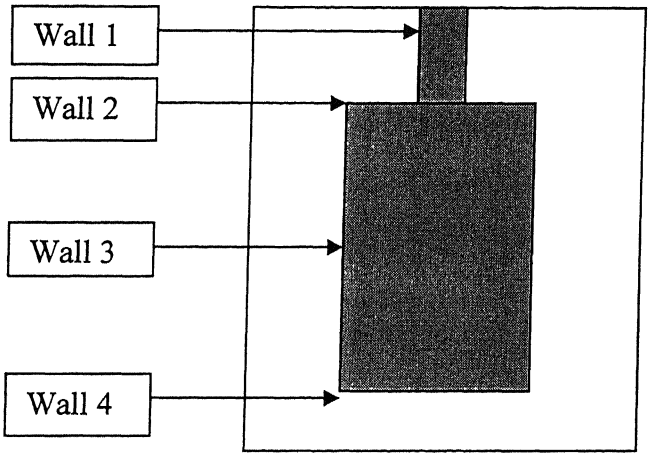

Figure 2.8: Schematic diagram showing various surfaces of the rotating assembly

	Surface	Surface Area, m^2	Surface Area fraction Shear stress, N/m^2	% Contribution
Wall 1	Curved surface: shaft	9.113619×10^{-5}	0.04039	3.544
Wall 2	Upper planar surface: spindle	9.256×10^{-4}	0.0684	6.000
Wall 3	Curved surface: spindle	1.0058×10^{-3}	0.95403	83.729
Wall 4	Lower planar surface: shaft	1.06426×10^{-4}	0.0766	6.722
NET		***1.223744×10^{-3}***	***1.13942***	***~100***

Table 2.6: Numerically predicted wall shear stress on various surfaces of the rotating assembly and their proportionate contribution to the net shear stress

2.1.6.2 Estimation of Cell parameter (C_s)

Based on the computed shear stress values reported in Table 2.6, attempts were made to calculate the viscosity cell parameter (C_s) mentioned earlier. The cell parameter is given by the formula:

$$C_s = \frac{1}{2\pi k^2 R^2 L} \tag{2.5}$$

This is commonly stated as inverse of surface area multiplied by the distance. As already stated in the Section 2.1.2, the value of the C_s for the viscometer under consideration is 140530 m^{-3} as reported in the original reference. Numerically predicted value of the cell parameter was found to be equal to 147136 m^{-3}, which is in good agreement with the reported value.

2.2 PROBLEM 2 – MEASUREMENT OF VISCOSITY OF CaO – FeO SLAGS IN A ROTATING VISCOMETER

2.2.1 Case for Simulation

In this part of the present study, the work done by the Wright and coworkers [32] on the determination of viscosity of CaO – FeO slags with and without spinel particles at a temperature of 1553 K has been considered. Similar to their previous work [30], the viscosity values were measured for the various speeds of rotation for each specific composition of the melt. The schematic of the rotating viscometer used in their study is shown together with all principal dimensions in Figure 2.9. From the literature, the average viscosity of the slag was taken to be 0.065 Pa.s and the density of the slag equal to 3850 Kg/m^3. The model configuration and the boundary conditions applied have been identical to those considered for problem 1 enumerated already and consequently not reported here.

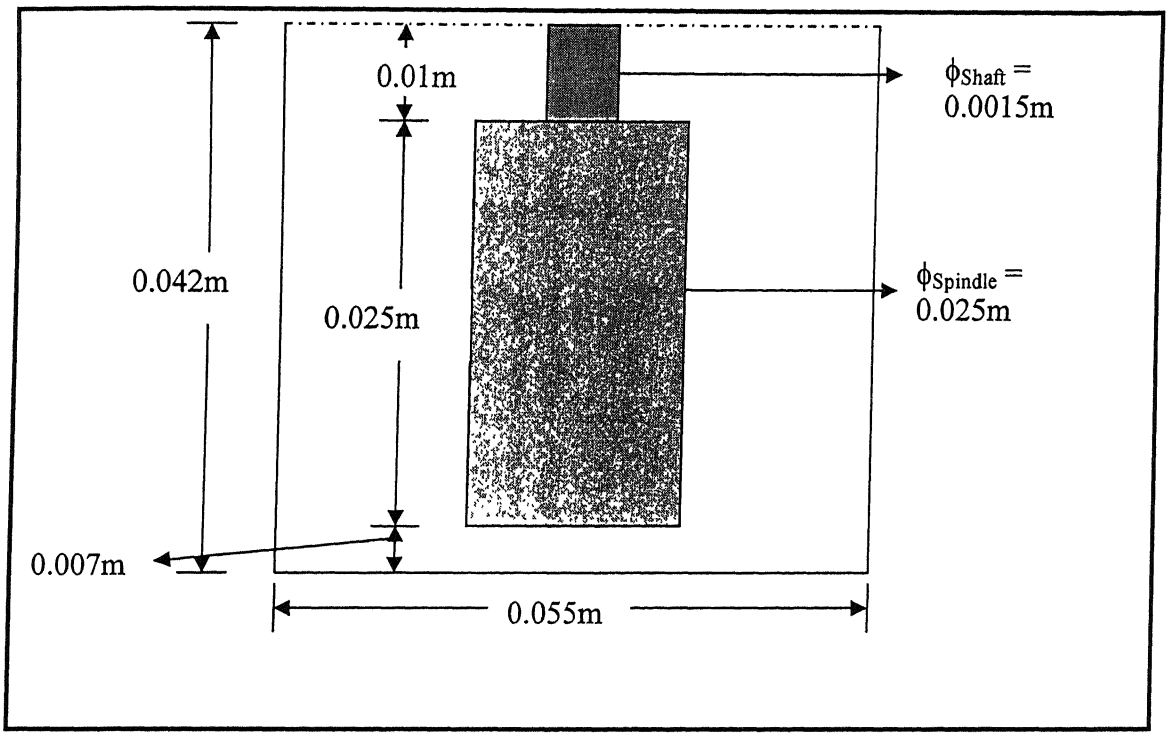

Figure 2.9: Schematic diagram of the viscometer II with principal dimensions

It is to be noted that without the value of C_s explicitly specified, the representative value of shear stress cannot be determined from the measured torque data. Consequently, for the present purpose, since the cell parameter, C_s, value was not given in the original paper, it was determined from the experimental configuration using Equations (2.2) and (2.4). On the basis of such, an average value of the cell parameter is deduced. The shear stress value is deduced from Equation (2.4). The experimental data on speed, torque and viscosity together with the estimated values of shear stress and the viscosity cell parameter are summarised in Table 2.7.

Speed, rpm	Viscosity, Pa.s.	Torque, N.m	C_s, m^{-3}	Estimated Shear stress, N/m^2
20	0.054	9.26338E-06	30779.28	0.284347
30	0.054	1.43161E-05	29874.01	0.439446
50	0.064	2.65269E-05	31846.87	0.814268
60	0.056	2.94744E-05	30095.29	0.904742
100	0.06	5.43171E-05	29162.11	1.66731

Table 2.7: Reconstructed data from the experimental measurements and estimated shear stress

It is important to mention that, in their paper [32] neither the value of cell parameter nor the depth of immersion of the spindle in the bath was mentioned. In addition, the conversion factor for the percentage torque to full scale torque has also not mentioned in their work.

2.2.2 Comparison of Shear Stress: Estimated vs. Numerical

The comparison of numerically predicted and experimentally determined shear stress is shown in the Table 2.8 and in the Figure 2.10. In these computations, the depth of immersion of the shaft is taken be 10 mm. The results show that there is some discrepancy between the experimental and predicted shear stress. The discrepancy while acceptable at low rpm is significant at high rpm. The reasons for such deviation is likely to be due:

1. unavailability of the depth of immersion data,
2. uncertainty in the estimation of the viscometer cell parameter and
3. On set of transition or turbulence flow conditions (Re>> 1, see later) particularly for higher rotational speed of the spindle.

These are discussed in the following section in detail.

Speed, rpm	Estimated Shear stress, N/m^2	Numerical Shear stress, N/m^2
20	0.284347	0.34227
30	0.439446	0.55578
50	0.814268	1.2172
60	0.904742	1.4714
100	1.66731	3.3619

Table 2.8: Comparison of shear stress: Estimated and Numerical

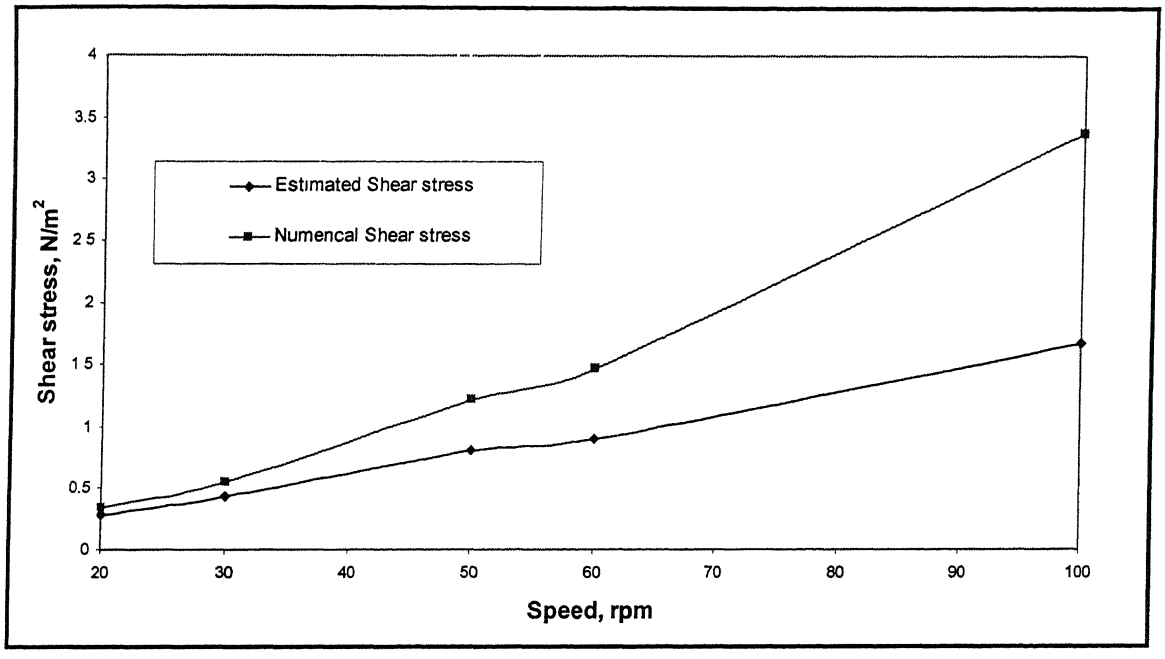

Figure 2.10: Comparison of the shear stress: Estimated and Numerical

2.2.3 Analysis of Uncertainty in predicted Results

2.2.3.1 Grid configuration

As our first step, the grid independency of the computed results was analyzed. It was noted that the grid configurations applied produced essentially grid independent results. This is shown in Figure 2.11. Consequently, nodal configuration cannot be attributed to the discrepancy is illustrated in Figure 2.10.

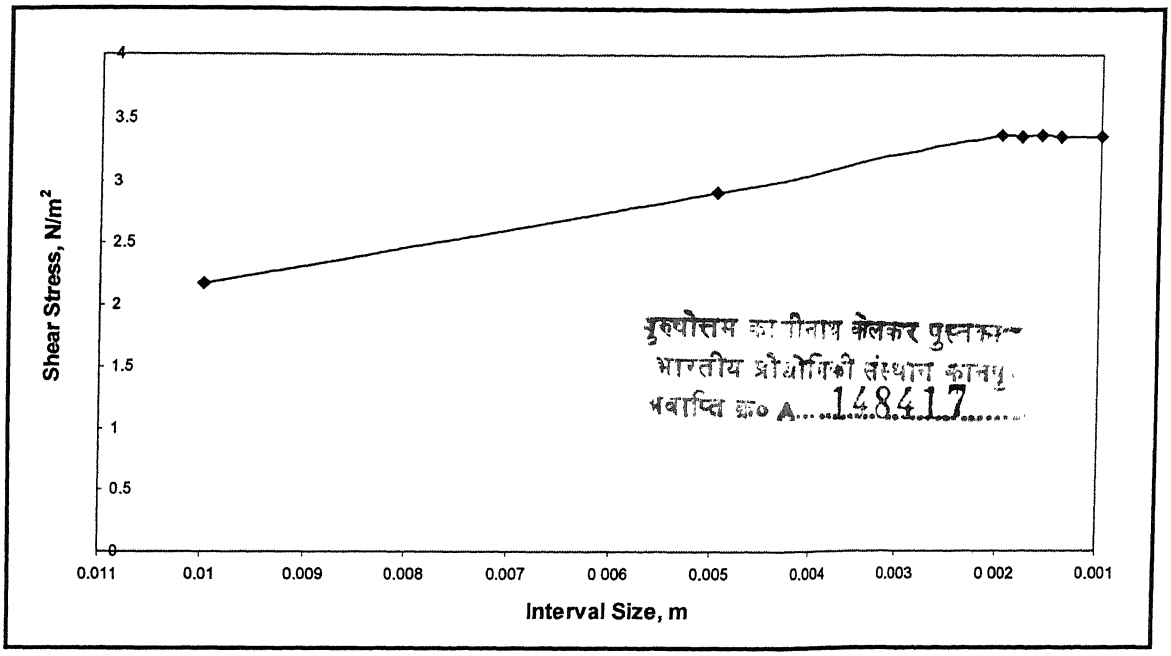

Figure 2.11: Grid independence test

2.2.3.2 Role of vessel taper

The crucible used in the experimental work was slightly tapered. The effect of the taper with a taper angle of 2.71° on the computed results is shown in the Table 2.9 for the speeds of 20, 50 and 100 rpm. The results show that the effect of taper is negligible which was observed in the context of the earlier problem.

Speed, rpm	Estimated Shear stress, N/m^2	Numerical Shear stress, N/m^2 without taper	Numerical Shear stress, N/m^2 with taper
20	0.2843	0.3422	0.3460
50	0.8142	1.2172	1.2199
100	1.6673	3.3619	3.3213

Table 2.9: Comparison of shear stress: with and without taper of the outer crucible

2.2.3.3 Cell parameter

As stated earlier, the average value of the cell parameter is used in calculating the shear stress. The effect of this is analyzed by embodying individual cell parameter in the

calculation scheme as well. The results are shown in the Table 2.10 for the speeds of 20, 50 and 100 rpm indicate that predicted results are not critical to the precise values of the viscometer cell parameter. The uncertainty in the viscosity cell parameter value is perhaps not the reason for the discrepancy illustrated in Figure 2.9.

Speed, rpm	Estimated Shear stress, N/m^2	Numerical Shear stress, N/m^2 with average C_s value	Individual C_s, m^{-3}	Numerical Shear stress, N/m^2 with individual C_s value
20	0.2843	0.3422	30779	0.3369
50	0.8142	1.2172	31846	1.2413
100	1.6673	3.3619	29162	3.2842

Table 2.10: Comparison of shear stress: with average and individual C_s value

2.2.3.4 Depth of Immersion (DOI)

As mentioned already, the depth of immersion of the spindle into melt was not stated explicitly in the original paper. It was however mentioned [32] that various depths of immersions such as 5, 10, 15 and 20 mm were applied. Consequently, a sensitivity analysis was carried out embodying plausible values of depth of immersion of the spindle. Results presented in Table 2.11 clearly show that the discrepancy between predicted and experimental shear stress cannot be attributed to the uncertainty associated with the depth of immersion of the spindle.

Speed, rpm	Estimated Shear stress, N/m^2	Numerical Shear stress, N/m^2 DOI = 10 mm	Numerical Shear stress, N/m^2 DOI = 5mm
20	0.2843	0.3422	0.3255
50	0.8142	1.2172	1.1146
100	1.6673	3.3619	3.1096

Table 2.11: Comparison of shear stress for the different depths of immersion (5 and 10 mm)

The foregone discussion clearly indicates that the discrepancy between predicted and experimental system, which albeit has a systematic trend (as seen from Figure 2.9) is not due to uncertainty associated with the value of viscosity cell parameter or the depth of immersion of the spindle. Similarly errors associated with experimental measurements are also unlikely to be the reason since the deviation between the two set of data is systematic rather than scattered. It is not therefore unlikely that the present model is inadequate to simulate the hydrodynamics in the system realistically. Towards this some additional considerations are presented in the following section

.

2.2.3.5 Critical Speed and Onset of Turbulence

In the analysis presented above, the flow within the viscometer has been assumed to be laminar. One would, however, note that the set of speeds used for problem 1 are significantly smaller than those considered for problem 2. Furthermore, as seen from Figure 2.9, the deviation between experimental data and predicted results tend to increase as the rotational speed of the spindle is increased. To assess the role of transition flow conditions on the predicted results, the condition of transition from laminar to the turbulent for the present geometry is considered and represented as [23]:

$$\left(\frac{\Omega_i \rho R_{spindle}^2}{\mu}\right)_{trans} = \frac{41.3}{\left(1-\frac{R_{spindle}^2}{R_{crucible}^2}\right)^{3/2}} \qquad (2.6)$$

The left hand side of the Equation (2.6) is the Reynolds number (N_{Re}) of the flow. For the various speeds of rotation, the N_{Re} value is calculated and shown in Table 2.12. At the highest speed of rotation, the value of Reynolds number as estimated from Equation 2.6 is equal to 102.52 and for problem 1 the value is 44.3. Such estimates clearly indicate that flow is transitional in the system rather than laminar. Consequently, it appears that for higher speed of rotation of the spindle, the application of a laminar flow model is questionable. Indeed true laminar conditions are likely to prevail provided Reynolds number has a value of the order of unity or less. This explains that with a laminar flow model, agreement between experimental and predicted shear stress is

expected to be adequate only for low rotational speed (as has been in Problem 1 in Table 2.13) and not for higher speed (e.g., the latter case, problem 2).

Speed in rpm	Speed, rad/s	Viscosity, Pa.s	N_{Re}
20	2.0944	0.054	23.33
30	3.1416	0.054	35
50	5.2359	0.064	49.21
60	6.2831	0.056	67.41
100	10.4719	0.06	105

Table 2.12: Estimated Reynolds number for various speeds of rotation for problem2

Speed in rpm	Speed, rad/s	Viscosity, Pa.s	N_{Re}
2	0.2094	2.59	0.007409
2.5	0.2618	2.42	0.009912
3	0.3141	2.59	0.011113
4	0.4188	2.26	0.016981
5	0.5235	2.24	0.021416
10	1.0472	2.2	0.043611
12	1.2566	2.16	0.053302

Table 2.13: Estimated Reynolds number for various speeds of rotation for problem1

2.2.4 Numerical Simulation for a Higher Viscosity Fluid

The numerical simulations for the higher viscosity fluid i.e. liquid with the 5% solid particles were also computed at lower rpm and the results of estimated and computed shear stresses are shown in the Table 2.14 and Figure 2.12. Once again very reasonable agreement between prediction and experiment is readily evident. The extent of non agreement seems to manifest more as the rotational speed increases.

Speed, rpm	Viscosity, Pa.s	Estimated Shear stress, N/m^2	Numerical Shear stress, N/m^2	Numerical Shear stress, N/m^2 with taper
3	0.68	0.51698	0.5708	0.5609
6	0.44	0.6849	0.7402	0.7494
10	0.42	1.0856	1.1806	1.1951
12	0.37	1.1503	1.2506	1.2660
20	0.35	1.8223	1.9843	2.0088

Table 2.14: Comparison of Experimental and predicted shear stress for a higher viscosity fluid: Estimated, Numerical shear stress without taper

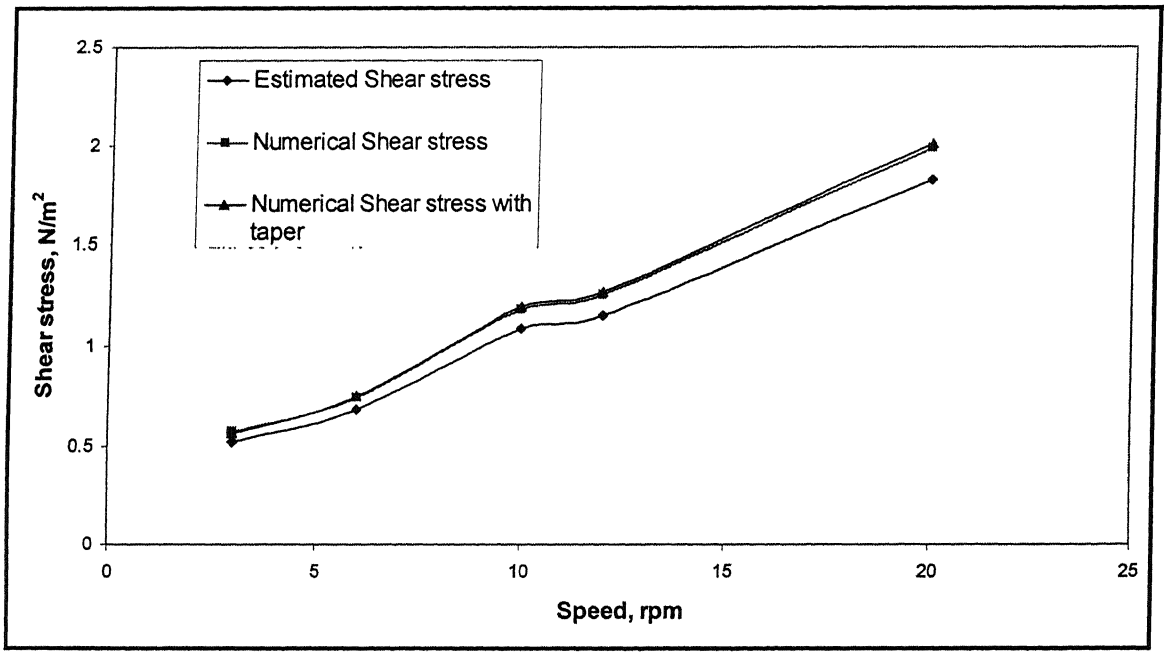

Figure 2.12: Comparison of shear stress for a higher viscosity fluid: Estimated, Numerical (with taper) and Numerical (without taper)

The effect of the depth of immersion of the spindle is also studied together with the effect of taper. The results were tabulated in the Table 2.15 and Figure 2.13. The results show that agreement between measured and predicted shear stress is marginally better if 10cm depth of immersion is used in lieu of 5 cm.

Speed, rpm	Viscosity, Pa.s	Estimated Shear stress, N/m^2	Numerical Shear stress, N/m^2 DOI = 10mm	Numerical Shear stress, N/m^2 DOI = 5mm	Numerical Shear stress, N/m^2 DOI = 5mm with taper
3	0.68	0.51698	0.5708	0.5559	0.5617
6	0.44	0.6849	0.7402	0.7208	0.7284
10	0.42	1.0856	1.1806	1.1496	1.1617
12	0.37	1.1503	1.2506	1.2177	1.2305
20	0.35	1.8223	1.9843	1.9312	1.9515

Table 2.15: Comparison of experimental and predicted shear stress for a higher viscosity fluid for two different values of depth of immersion

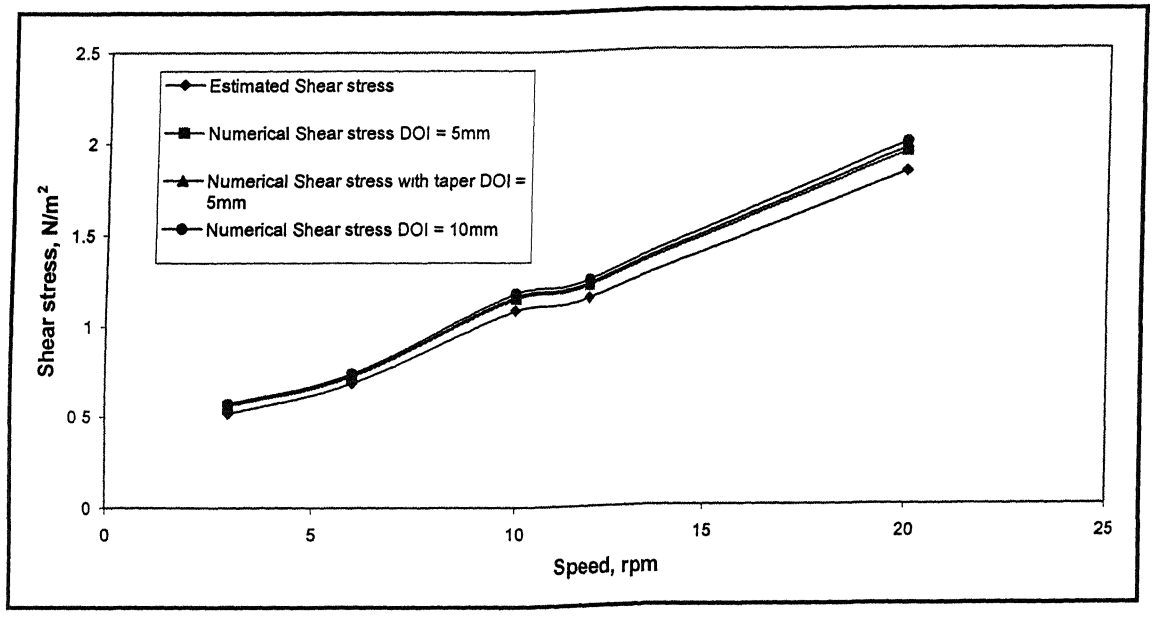

Figure 2.13: Comparison of shear stress for a higher viscosity fluid: The influence of geometrical parameter (Depth of immersion and crucible taper)

CHAPTER 4

CONCLUSIONS

Numerical simulation of fluid flow phenomena in rotating viscometer was carried out and the shear stress values for various speeds were computed. Extensive comparison was also made between computational results and experimental measurements. In the present work, the effect of the crucible taper, contribution of the shaft to the overall shear stress and the importance of the cell parameter and depth of immersion data were all studied computationally. From the present study, the following conclusions have been drawn.

- The present work has demonstrated that uni-dimensional flow theory coupled with a properly calibrated viscometer cell parameter (C_s) is adequate as far as measurement of viscosity in rotating viscometer is concerned.

- This approach also leads to sufficiently accurate estimates of shear stresses acting on the viscometer shaft and spindle.

- The three dimensional study carried out has further confirmed that estimates of shear stress thus derived is truly equivalent to the one acting on the rotating assembly (shaft and spindle) of the viscometer.

- The effect of the crucible taper in the viscometer geometry is negligible as far as measurement of viscosity is concerned. This justifies the approximation of the crucible as a regular cylindrical shaped vessel in the numerical as well as analytical treatment of the subject.

- The contribution of the shaft is significant and therefore cannot be ignored in the numerical formalism if shear stresses valued are to be predicted accurately.

CHAPTER 5

RECOMMANDATIONS FOR THE FUTURE WORK

The following recommendations have been made for future work.

- Since Fluent has been shown to predict hydrodynamics in the rotating viscometers fairly accurately, consequently, many fluid flow studies in the area of steelmaking can be attempted through Fluent. These include, flow in continuous casting molds, BOF, ladles, tundishes and so on.

- A coupled experimental cum computational work may be initiated in which rotating viscometers together with fluent based models can be applied to develop fundamental quantitative understanding of slag – metal interactions in high temperature flow systems.

REFERENCES

1. Olusegan J. Ilegbusi, Manabu Iguchi, Walter Wahnsiedler: Mathematical and Physical Modelling of Materials Processing Operations, Chapman & Hall/CRC, 2000.
2. J.K. Brimacombe: Int. Conf. on 'Progress in Metallurgical Research: Fundamental and Applied Aspects,' Feb 11 – 15, 1985, IIT, Kanpur
3. Julian Szekely: Materials and Metallurgical Transactions B, Volume – 19B, August 1988, 525.
4. T. Lehner and J. Szekely: Scandinavian Journal of Metallurgy, 19, 1990, 174
5. http://www.fluent.com/solutions/index.htm
6. Aniruddha Mukhopadhyay: Fluent Inc, www.fluent.com/solutions/articles/ja143.pdf
7. M. Salcudean and R.I.L. Guthrie: Materials and Metallurgical Transactions B, Vol.9B,1978, 673
8. N.El-Kaddah and J. Szekely: Ironmaking and Steelmaking, Volume 6, 1981, 269.
9. M. Salcudean, K.Y.M. Lai and R.I.L. Guthrie: Canadian Journal of Chemical Engineering, Volume 63, 1985, 51.
10. D.Mazumdar and R.I.L.Guthriie: Applied Mathematical Modelling, Volume 10, 1986, 25.
11. F.B. Boysan and S.T. Johansen: Materials and Metallurgical Transactions B, Volume19B, 1987,755.
12. M.P. Scwarz and W.J. Turner: Applied Mathematical Modelling, Volume 12, 1988,273.
13. Illegbussi and J. Szekely: ISIJ International, Volume 29, 1989, 1031.
14. H. Turkoglu and B. Farouk: ISIJ International, Volume 31, 1993, 1371.
15. S. Chakravorty and Y. Sahai: Metall. Trans., Volume.23B, 1992,488.
16. T. Ishi, S.S. Sazhim and M. Makhlouf: Ironmaking and Steelmaking, Volume 23, 1996,267.
17. D.Y. Sheng, C.S. Kim, J.K. Yoon and T.C. Hsiao: ISIJ International, Volume 8, 1998, 851.

18. H. Bai and B.G. Thomas: Metallurgical and Materials Transactions B., Volume 32B, 2001,269.
19. A. Ramos-Banderas, R. Perez-sanchez, R.D. Morales and J. Palafox-Ramos: Metallurgical and Materials Trans. (in Press).
20. Gordon A. Irons: Second International Conference on CFD in the Minerals and Process Industries, CSIRO, Dec 6 – 8, 1999, Melbourne.
21. FLUENT 6.1 Documentation CD, Fluent Inc, Lebenon, NH, 2003
22. GAMBIT 2.1 Documentation CD, Fluent Inc, Lebenon, NH, 2003
23. R.B. Bird, W.E. Stewart and E.N. Light foot: Transport Phenomena, John Wiley and Sons, New York, 1960
24. J. Kowalczyk, W. Mroz, A. Warczok and T.A. Utigard: Materials and Metallurgical Transactions B, Volume 26B, 1995, 1217.
25. S. Hara, M. Kitamura, and K. Ogino: ISIJ International, Volume 30, 1990, 714.
26. T.P. Battle and J.P. Hager: Materials and Metallurgical Transactions B, Volume 21B, 1990, 501.
27. P.G. Jonsson, L. Jonsson and D. Sichen: ISIJ International, Volume 37, 1997, 484.
28. F.-Z.Ji, D.Sichen, K.C. Mills and S. Seetharaman: Ironmaking and Steelmaking, Volume 25 (4), 1998, 309.
29. F. Shabazian, D. Sichen, K.C. Mills and S. Seetharaman: Ironmaking and Steelmaking, Volume 26 (3), 1999, 193.
30. S. Wright, L. Zhang, S. Sun and S. Jahanshahi: Materials and Metallurgical Transactions B, Volume 31B, 2000, 97.
31. K. Nakashima and K. Mori: Materials and Metallurgical Transactions B (in press).
32. S. Wright, L. Zhang, S. Sun and S. Jahanshahi: Journal of Non crystalline Solids, Volume 282, 2001, 15.